Diamond & Related Materials 150 (2024) 111668

Contents lists available at ScienceDirect

Diamond & Related Materials

journal homepage: www.elsevier.com/locate/diamond

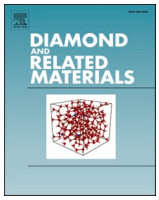

MAX phase borides, the potential alternative of well-known MAX phase carbides: A case study of V_2AB [A = Ge, P, Tl, Zn] via DFT method

M.A. Ali [a,*], S. Nath [a], S. Mahmud [a,b], N. Jahan [a], M.M. Uddin [a]

[a] Advanced Computational Materials Research Laboratory, Department of Physics, Chittagong University of Engineering and Technology (CUET), Chattogram 4349, Bangladesh

[b] Department of Electrical and Electronic Engineering, Jatiya Kabi Kazi Nazrul Islam University (JKKNIU), Mymensingh 2224, Bangladesh

ARTICLE INFO

Keywords:
DFT
MAX phase
Electronic properties
Mechanical properties
Thermal properties

ABSTRACT

This study predicted four new MAX phase borides via the DFT method, with a comprehensive and thorough approach. The stability of the predicted phases has been thoroughly studied using formation energy, phonon dispersion curve (PDC), and elastic constants (C_{ij}). The metallic nature of the studied phases is confirmed through the computation of the electronic band structure and density of states (DOS). Their bonding nature is disclosed using the partial density of states, Mulliken population analysis, and charge density mapping. The mechanical behavior is investigated in depth by calculating elastic constants, elastic moduli, Poisson's & Pugh ratio, machinability index, and Vickers hardness. Different anisotropic indices are also computed to demonstrate the elastic anisotropy. The Debye temperature (Θ_D), Grüneisen parameter (γ), phonon thermal conductivity (k_{ph}), minimum thermal conductivity (k_{min}), thermal expansion coefficient (*TEC*), and melting temperature (T_m) are all calculated, and the suitability of the studied phases as thermal barrier coating (TBC) materials has been discussed. Finally, the optical constants are calculated and analyzed, further certifying the metallic nature of the herein-studied phases. The reflectivity spectra of all the herein selected compounds reveal their potential as coating materials to lessen solar heating. Among the studied phases, V_2PB exhibits the best thermo-mechanical properties for potential applications in diverse fields, such as structural components and TBC materials. The potential applications of our findings are vast, and the obtained results reveal that the predicted phases are indeed potential alternatives to their counterpart carbides.

1. Introduction

The MAX phases are a remarkable type of nano-laminated layered solids. They possess a unique combination of properties, making them quite fascinating. The materials are stiff and lightweight, yet they are still easily machinable. They are also oxidation and creep-resistant, in addition to being metallic conductors and exceptionally resistant to thermal shock [1–5]. The standard formula for MAX Phases is $M_{n+1}AX_n$, where M stands for an early transition metal, A is an element from the A-group, and X is either C or N. Interestingly, MAX Phase materials uniquely blend ceramic and metallic characteristics [1–5]. The metallic attributes, such as mechanical strength, metallic conductivity, and easy machinability, and the ceramic attributes, such as high-temperature sustainability, corrosion, and oxidation resistance, make the MAX phase materials one of the focused and researched materials [1,2,5]. Due to the MAX phase's benefits across various sectors, 342 MAX phases are known, and 182 are also expected to be synthesizable [5].

The diversity of the MAX phase's members for the X element was limited to C or N, even though they mature by tuning the M or A elements. As a result, an expansion of the X elements can lead to the addition of numerous additional compounds as MAX phase members. It is fantastic news that the B/P atom, reported by the researchers, can replace the X (C/N) element [5]. Several reports are available that deal with the MAX phase borides. For example, the MAX family has been extended by the synthesis of MAX phase borides: M_2SB (M = Zr, Hf, Nb) by Rackl et al. [6,7]. The first work published on MAX phase borides has been done by Khazaei et al. [8], wherein M_2AlB (M = Sc, Ti, Cr, Zr, Nb, Mo, Hf, and Ta) borides have been reported as stable materials along with their electronic and mechanical properties. A lower ductility was claimed for the borides compared to the carbide phases. Additionally, Sc_2AlB was found to be mechanically unstable, while Ta_2AlB has the best potential for forming a 2D nano-sheet. G. Surucu [9] studied M_2AB (M =

* Corresponding author.
E-mail address: ashrafphy31@cuet.ac.bd (M.A. Ali).

https://doi.org/10.1016/j.diamond.2024.111668
Received 2 August 2024; Received in revised form 6 October 2024; Accepted 13 October 2024
Available online 21 October 2024

Ti, Zr, Hf, and A = Al, Ga, In) boride phases by exploring their structural, electronic, mechanical, phonon, and thermal properties. Three Hf-based MAX phases [Hf_2XY (X = Al, Si, P, and Y = B, C, N)], along with carbides and nitrides, were explored by Aydin et al. [10] where the boron and phosphorus-containing compounds were considered for the first time. It was observed that phases containing nitrogen have lower cohesive energy compared to phases containing boron. Additionally, both Hf2AlB and Hf2SiB were reported to be dynamically unstable. Ali et al. [11] studied the unexplored properties such as dynamic stability, mechanical anisotropy, thermodynamic, and optical properties of the synthesized M_2SB (M = Zr, Hf, Nb) borides. The electronic, thermal, mechanical, and optical properties of Hf_2AB (A=Pb, Bi) phases were investigated by Hossain et al. [12,13] in ambient conditions as well as under high pressure. The full-potential linearized augmented plane wave (FP-LAPW) method was applied to explore M_2AC and M_2AB (M = Nb or Mo, A = Al or Ga) MAX phases by Essaoud et al. [14]. In their research, Rana et al. [15] reported the M_2GaB [M = Sc, V, Nb, Ta] phases as potential candidates of the MAX phase family. Additionally, Islam et al. [16] further investigated the unexplored properties of M_2GaB (M = Ti, Zr, and Hf) and, for the first time, predicted the existence of the Mo_2GaB boride phase. Recently, Zr_2SeB, Hf_2SeB [17], and Hf_2TeB [18] phases were synthesized, which were then further studied by Islam et al. [19] theoretically. Zhou et al. [20] predicted nine new MAX phase borides M_2AB (M = Zr, Hf, Nb, A = P, As, and Sb). The Zr_2SeB phase was also studied theoretically by Bai et al. [21]. In a more recent study, Akhter et al. [22] explored two new Sc-based MAX phase borides. A first-time report of the 312 MAX phase borides, M_3GaB_2 (M = Ti, Hf), was carried out by Ishtiaq et al. [23].

In the cases mentioned above, the authors have shown that the boride phases can be used as an alternative to the previously known carbide phases. Some MAX-phase borides exhibit improved thermo-mechanical properties and are superior to MAX-phase carbides. This prospect inspires us to extend the MAX phase family by exploring more borides phases, so we have selected the titled borides for the current project. Therefore, V_2AB [A = Ge, Tl, P, Zn] borides have been studied using DFT, considering their structural, electronic, mechanical, optical, and thermal properties. The study revealed that V_2PB would be an effective material for thermal barrier coatings (TBC) due to its very low weight, reasonably high elastic moduli, high melting point, very low minimum thermal conductivity, and good coefficient of thermal expansion.

2. Computational methodology

Physics and materials science researchers have paid substantial attention to the DFT-based ab-initio calculations [24,25]. A widely used BFT-based code, Cambridge Serial Total Energy Package (CASTEP) [26,27], was considered to calculate the physical properties of the studied MAX phases. The exchange-correlation energy has been described by the Perdew–Burke–Ernzerhof (PBE) typed generalized gradient approximation (GGA) [28]. Ultrasoft pseudopotentials (USP), developed by Vanderbilt (1990), were selected to converge the plane wave for transition metals [29] during the calculation of the electron-ion interaction. The USP method relaxes the norm-conservation constraint and describes the difference in charge densities between the all-electron and pseudo-orbitals using a few localized augmentation functions, which enables low cutoff energy in a plane-wave basis setting. The optimized structure was obtained using the Broyden–Fletcher– Goldfarb–Shanno (BFGS) scheme [30]. All the calculations were performed using a k-point mesh of size 9 × 9 × 2 (Monkhorst–Pack schemes) [29] and a cutoff energy of 500 eV. The phonon dispersion curves were calculated using the finite displacement method. All other relevant equations and formalisms have been stated in the respective results and discussion sections.

3. Results and discussion

3.1. Structural properties and stability

In Fig. 1, the crystal structure of the ternary V_2AB MAX phase is depicted. This phase has a hexagonal structure with a space group P63/mmc, similar to other MAX compounds containing C or N [7,11,17,20,31–33]. Like other MAX phases [34], the compounds being studied also have two formula units, each containing eight atoms, with four atoms in each unit.

In the unit cell, the Wyckoff positions of the constituent atoms are as follows: V at 4*f* (0.3333, 0.6667, Z_M), Ge at 2*d* (0.3333, 0.6667, 0.75), and B at 2*a* (0,0,0) sites. The important structural parameters of V_2AB MAX phase borides are given in Table 1, which includes the lattice constants (*a*, *c*), internal parameter (z_M), and *c*/*a* ratio of the titled phases. A comparison is not feasible as these phases are being reported for the first time.

Stability checking is crucial for predicting any phases. This study calculated the formation energy, phonon dispersion curve (PDC), and elastic constants to achieve this. Table 1 lists the calculated formation energy of the titled phases using the formalism, which have been used by many researchers to predict new materials [35,36], particularly MAX phases [15,37–41].

$$E_{for}^{V_2AB} = \frac{E_{total}^{V_2AB} - \left(xE_{solid}^{M} + yE_{solid}^{Ga} + zE_{solid}^{B}\right)}{x+y+z}; A = \mathrm{Ge, P, Tl, Zn}$$

Here, $x = 4$, $y = 2$, and $z = 2$ represent the atomic numbers of V, A, and B present in the unit cell and $E_{total}^{V_2AB}$, E_{solid}^{M}, E_{solid}^{Ga}, and E_{solid}^{B} are the corresponding energies of V_2AB compounds and V, A, and B solids (with stable structures), respectively.

The V_2GeB, V_2PB, V_2TlB, and V_2ZnB have formation energies of −0.72, −0.86, −042, and − 0.54, respectively. Therefore, the studied phases are thermodynamically stable. After confirming the thermodynamic stability, we have calculated the phonon dispersion curve (PDC). The PDC is widely used to check the stability of materials under varying conditions, such as temperature and pressure. In this case, the PDCs of all the phases exhibited positive frequencies. The presence of negative

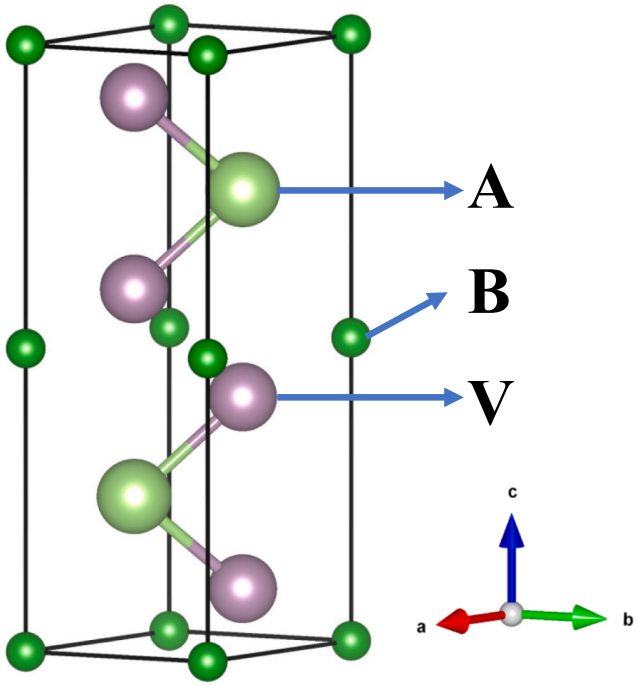

Fig. 1. The schematic unit cell of V_2AB (A = Ge, P, Tl, Zn) borides.

Table 1
Calculated lattice parameters (a and c), internal parameter (Z_M), and formation energy (E_F) of V_2AB (A = Ge, P, Tl, Zn) borides.

Phases	a (Å)	c (Å)	Z_M	c/a	E_F (eV)
V_2GeB	3.0333	12.3732	0.5938	4.0791	−0.86
V_2PB	3.1226	10.9192	0.6051	3.4968	−0.97
V_2TlB	3.1581	13.6334	0.5763	4.3169	−0.42
V_2ZnB	2.9716	13.2687	0.5870	4.4651	−0.54

frequency certifies instability, thereby indicating the non-existence of any imaginary frequency in the considered Brillouin zone, which in turn confirms the dynamical stability of the titled compounds.

Furthermore, the PDCs provide additional information that can be used to analyze the vibrational characteristics of the titled compounds. The 211 phases, consisting of 8 atoms, should have 24 phonon modes, including three acoustic and 21 optical modes. The high-frequency optical modes exhibit less dispersion compared to the lower-frequency range. The low-frequency optical modes hybridize with the acoustic modes, albeit at a distance from the G point compared to other symmetry points. Additionally, the highest optical modes are separated by a phononic band gap, which is not observed in the low-frequency optical modes and acoustic modes. The dispersion of acoustic branches varies due to the hybridization with the low optical modes. The weaker the hybridization between acoustic and optical modes, the more dispersive the acoustic modes and the greater the phonon contribution to the lattice thermal conductivity [42,43]. Among the 21 optical modes, there are six IR-active, seven Raman-active, and eight silent modes. The optical phonon modes at the Brillouin zone center can be represented by the following groups:

$$\Gamma_{opt.} = 2A_{2u} + 4E_{1u} + 2E_{1g} + 4E_{2g} + A_{1g} + 2B_{1u} + 2B_{2g} + 4E_{2u}$$

where A_{2u} and E_{1u} are IR active modes, A_{1g}, E_{1g}, and E_{2g} are Raman active modes and B_{1u}, B_{2g} and E_{2u} are silent modes [44,45]. The modes are presented in Table 2.

The nature of optical anisotropy can also be understood from the difference between the highest transverse optical modes (TO) and longitudinal optical modes (LO). For example, the calculated optical anisotropy [$\nu_{TO}(A_{2u})$- $\nu_{TO}(E_{1u})$] is 130.00, 59.36, 95.79, and 92.87 for V_2GeB, V_2PB, V_2TlB, and V_2ZnB, respectively. The optical anisotropy resulted is due to the atomic arrangement and atomic bonding within the structures [46].

The graph in Fig. 2 shows the phonon Density of States (PHDOS), which corresponds to the bands we obtained. The peaks in the PHDOS line up with the flat bands in the curves. We can see a decrease in the peaks due to the slopes of the bands. We've also included the partial PHDOS, which shows the contribution from different orbitals. The highest optical modes come from the B atoms, the lowest frequencies are from the A atoms (where A = Ge, Tl, Zn), and the mid-frequency range is contributed by the V atoms in the V_2GeB, V_2TlB, and V_2ZnB phases. In the V_2PB phase, the V atoms form the lowest acoustic branch, and the P atoms contribute to the mid-frequency range. This means that the A atoms play the most important role in determining the lattice thermal conductivity in the V_2GeB, V_2TlB, and V_2ZnB phases, while the V atoms mainly contribute to the thermal conductivity of the V_2PB phase.

3.2. Electronic properties and bonding nature

The electronic band structure, DOS, charge density mapping, etc., usually describe the electronic conductive nature of solids and electronic bonding within the solids. The band structures of the titled compounds are shown in Fig. 3, wherein overlapping of the conduction and valence band is seen, indicating the metallic nature of V_2AB [A = Ge, P, Tl, Zn] phases, like other MAX phase compounds (carbides) [47–49]. The band structure of the titled phases has demonstrated the anisotropic electronic conductivity. Within the Brillouin zone, the electronic paths Γ-A, H—K, and M-L are in the z-direction, whereas the paths A-H, K-Γ, Γ-M, and L-H are in the basal plane. The level of dispersion among these paths indicates the comparative electronic conductivity; the higher the dispersion, the lower the electronic conductivity. This characteristic results from differences in the effective electronic mass tensor along different directions [44]. Similar results have been published for many MAX phases [50–52]. As a result, a lower degree of electronic conductivity along the z-axis is observed compared to that in the basal planes. Atomic arrangement along the different axes is the same for cubic materials, which results in a typical isotropic nature. On the other hand, the atomic arrangement in the different directions is not the same for hexagonal or layered structured materials, causing an anisotropic behavior of electronic response, contribution as well and interaction also; this (anisotropic) nature of materials is crucially used in electronic devices

Table 2
Theoretical wave numbers ω and symmetry assignment of the IR-active and Raman-active modes of V_2AB [A = Ge, P, Tl, Zn) MAX phases borides.

Theoretical Mode symmetry	IR (V_2GeB)	Raman (V_2GeB)	Theoretical Mode symmetry	IR (V_2PB)	Raman V_2PB)	Theoretical Mode symmetry	IR (V_2TlB)	Raman (V_2TlB)	Theoretical Mode symmetry	IR (V_2ZnB)	Raman (V_2ZnB)
E1u	–	–	A2u	–	–	E1u	–	–	A2u	–	–
E1u	–	–	E1u	–	–	E1u	–	–	E1u	–	–
A2u	–	–	E1u	–	–	A2u	–	–	E1u	–	–
E2 g	–	109.18	E2u	–	–	E2 g	–	42.32	E2u	–	–
E2 g	–	109.18	E2u	–	–	E2 g		42.32	E2u	–	–
E2u	–	–	E2 g	–	188.99	E1u	71.84	–	E2 g	–	83.64
E2u	–	–	E2 g	–	188.99	E1u	71.84	–	E2 g	–	83.64
E1u	157.10	–	B1u	–	–	E2u	–	–	E1u	109.08	–
E1u	157.10	–	B2 g	–	–	E2u	–	–	E1u	109.08	–
B1u	–	–	E1 g	–	285.21	B2 g	–	–	B1u	–	–
B2 g	–	–	E1 g	–	285.21	B1u	–	–	B2 g	–	–
E2 g	–	245.27	E1u	333.53	–	A2u	167.36	–	A2u	201.95	–
E2 g	–	245.27	E1u	333.53	–	E2 g	–	236.28	E1 g	–	211.30
E1 g	–	255.04	E2 g	–	357.67	E2 g	–	236.28	E1 g	–	211.30
E1 g	–	255.04	E2 g	–	357.67	E1 g	–	242.25	E2 g	–	215.41
A2u	287.10	–	A1 g	–	392.85	E1 g	–	242.25	E2 g	–	215.41
A1 g	–	299.56	A2u	392.85	–	A1 g	–	294.24	A1 g	–	290.93
B2 g	–	–	B2 g	–	–	B2 g	–	–	B2 g	–	–
E2u	–	–	A2u	616.53	–	A2u	638.74	–	B1u	–	–
E2u	–	–	B1u	–	–	B1u	–	–	A2u	577.50	–
E1u	662.73	–	E2u	–	–	E2u	–	–	E1u	625.78	–
E1u	662.73	–	E2u	–	–	E2u	–	–	E1u	625.78	–
B1u	–	–	E1u	638.96	–	E1u	686.17	–	E2u	–	–
A2u	669.61	–	E1u	638.96	–	E1u	686.17	–	E2u	–	–

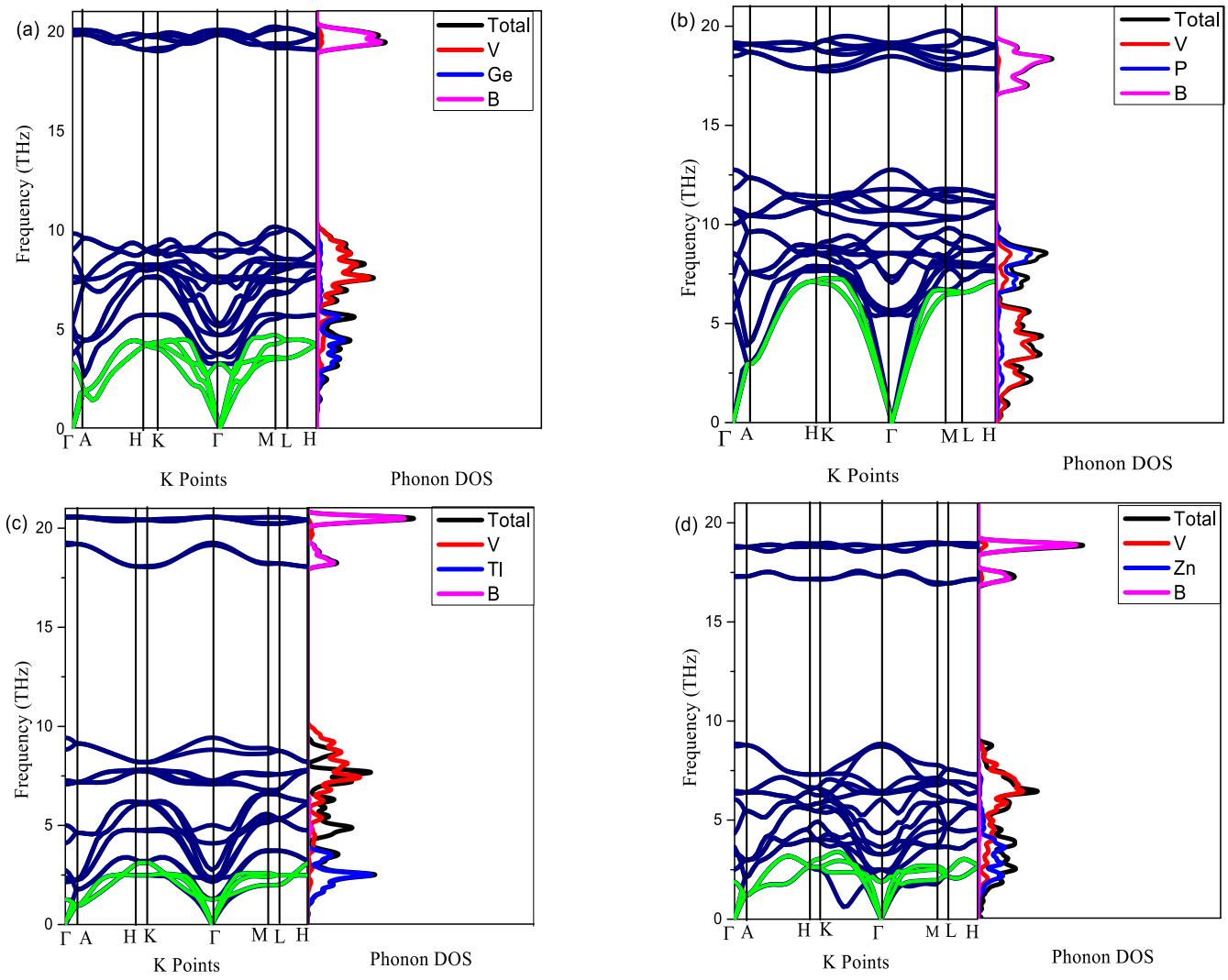

Fig. 2. Phonon dispersion curve and phonon DOS of (a) V_2GeB, (b) V_2PB, (c) V_2TlB, (d) V_2ZnB borides.

toward optimization of the performance or to attain particular functionalization.

The total and partial DOS of V_2AB [A = Ge, P, Tl, Zn] have been calculated to study the contribution from different states to the conductivity and hybridization among the different states. In Fig. 4, the computed DOSs are shown, with the Fermi level set at 0 eV and indicated by the dashed line. A reflection of the overlapping of valence and conduction band is seen by a distinct value of DOS at the Fermi level for each phase, which agrees well with band structure results. The V-*d* states predominantly contribute to the electronic conductivity at the fermi level, which is well consistent with traditional MAX phases. The bonding in the MAX phases is a combination of metallic, covalent, and ionic [53]. The presence of covalent bonding can be understood from the hybridization among the states, as shown in partial DOSs of Fig. 4. The strongest hybridization between B-*p* and V-*d* states is observed at around – 2.5 eV for each case, resulting in strong covalent bonding between V—B atoms. A comparatively weaker hybridization between A-*p* and V-*d* states is also noticed, indicating a covalent bonding that is weaker than the previous one. Metallic bonding is formed in the conduction band by V *d*-*d* orbitals.

The Mulliken atomic analysis, presented in Table 3, has demonstrated the existence of ionic bonding. The table shows the charge of constituent atoms in the respective phases. The V and A atoms carry positive charges, while the B atoms carry negative charges for each phase. This observation indicates a charge transfer from the positively charged atoms to the negatively charged ones, resulting in ionic bonding.

In the paragraphs above, we observed the metallic nature and a combination of covalent, ionic, and metallic bonding in the phases we studied. Now, let's examine how the strength of the bonding changes when we replace the A atom from Ge to P, P to Tl, and Tl to Zn. The change in bonding strength has been demonstrated by calculating the charge density mapping (CDM), as shown in Fig. 5. In CDM, the shape of the charges at the atomic position signifies the nature of atomic bonding. For example, the spherical shape around the atomic position signifies ionic bonding, while a distortion from the sphere indicates covalent bonding. The greater the distortion, the stronger the bonding. Let's now closely examine the positions of V and A [A = Ge, P, Tl, Zn] atoms. The most distorted charge distribution is observed for the V-P-V position, followed by V-Ge-V, V-Zn-V, and V-Tl-V. Thus, the bonding strength of the V-A covalent bonds is expected to follow the sequence: V-P > V-Ge > V-Zn > V-Tl. It is important to note that the V—B bonding strength is expected to be the same or nearly the same for each phase. Consequently, the hardness sequence is expected to be V_2PB > V_2GeB > V_2ZnB > V_2TlB, with a significantly large value of V_2PB. The hardness and elastic properties of V_2AB [A = Ge, P, Tl, Zn] have been presented in the following section.

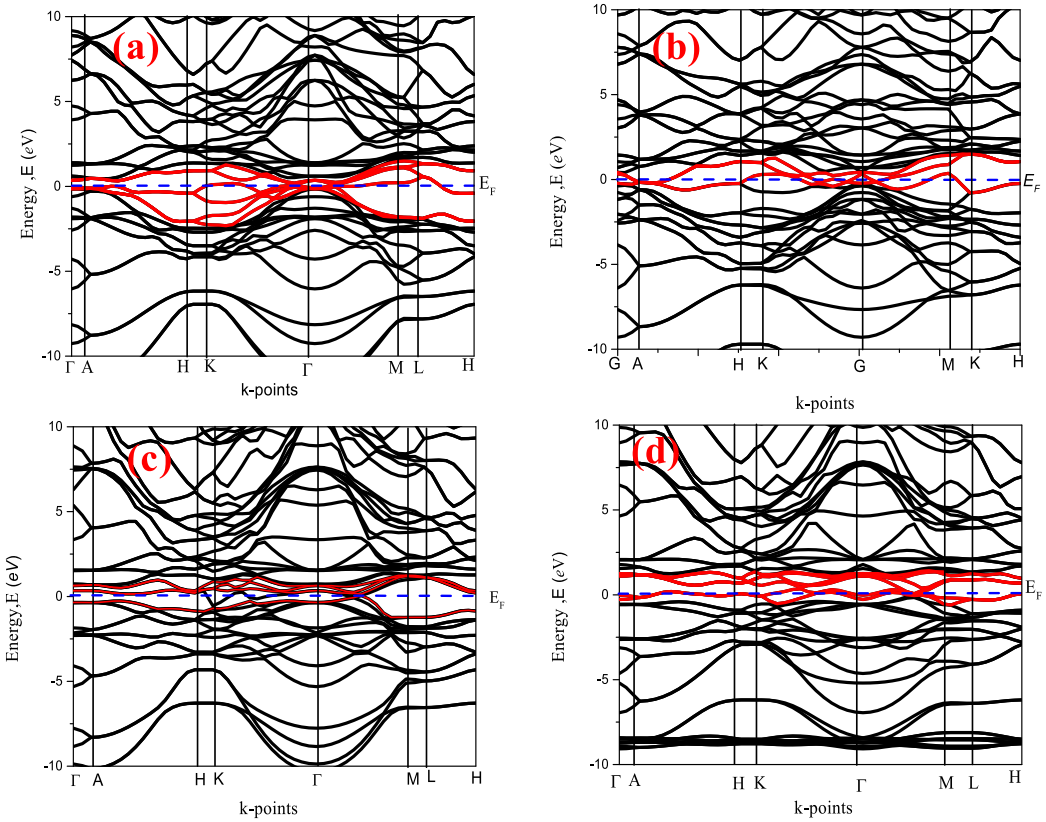

Fig. 3. Electronic band structure of (a) V_2GeB, (b) V_2PB, (c) V_2TlB, (d) V_2ZnB borides.

3.3. Elastic constants and mechanical behavior

A material's response to external forces can be understood by calculating its elastic constants, C_{ij}. The elastic constants also help to disclose a solid's mechanical behavior by calculating elastic moduli, brittleness/ductility, hardness parameters, machinability index, anisotropic level, propagation of elastic waves, etc. [41,54]. As the titled borides belong to the hexagonal system, there are five independent elastic constants and one dependent; a total of six elastic constants are there, as presented in Table 4. These constants were used to check the mechanical stability using the following conditions [55,56].

$$C_{11} > 0, C_{33} > 0, C_{44} > 0, C_{11} > C_{12}, (C_{11}+C_{12})C_{33} - 2C_{13}^2 > 0$$

The values of C_{ij} for all phases considered here satisfy the above-mentioned conditions. Thus, we claim that the tiled borides are mechanically stable.

These constants are used not only to check mechanical stability but also to infer some additional features of the considered compounds. For instance, the stiffness along the *a* and *c*-axes is measured by the values of C_{11} and C_{33}, whereas the constant C_{44} represents the resistance to shear deformation. The value of C_{44} is smaller than C_{11} and C_{33}, indicating that shear deformation is easier compared to deformation along the *a*/*c* direction. Moreover, the inequality of C_{11} and C_{33}, certifying a difference in stress along the *a* and *c*-axes, resulted in uneven bonding strength in these axes. Since these elastic constants are the basis of elastic moduli and mechanical properties of solids, anisotropy in the elastic properties is expected. Furthermore, these constants are used to calculate the elastic moduli by the following equations [57]:

$$B = (B_V + B_R)/2$$

here, $B_V = [2(C_{11}+C_{12}) + C_{33} + 4C_{13}]/9$ and $B_R = C^2/M$; $C^2 = (C_{11}+C_{12})C_{33} - 2C_{13}^2$;

$$M = C_{11} + C_{12} + 2C_{33} - 4C_{13}.$$

where B_V (Voigt bulk modulus [58]) and B_R (Reuss bulk modulus [59]) indicate the upper and lower values of B, respectively. *G* was computed using equations like *B*,

$$G = (G_V + G_R)/2$$

where, $G_V = (M + 12C_{44} + 12C_{66})/30$;

$$G_R = \left(\frac{5}{2}\right)[C^2C_{44}C_{66}]/[3B_VC_{44}C_{66} + C^2(C_{44}+C_{66})]; \quad C_{66} = (C_{11}-C_{12})/2.$$

Finally, *B* and *G* were used to compute the Young's modulus (*Y*) and Poisson's ratio (ν) as follows [60]:

$Y = 9BG/(3B+G)$ and $\upsilon = (3B-Y)/(6B)$

The computed values of *B*, *G*, *Y*, and ν are also present in Table 4. The *B* value indicates a material's ability to resist volume changes, while *G* represents its ability to withstand transverse (plastic) deformations. The highest *B* and *G* values are found for V_2PB, followed by V_2GeB. The *B* is the lowest for V_2TlB, but G is the lowest for V_2ZnB among the studied MAX phase borides. In this context, V_2TlB, with the lowest B value, exhibits higher compressibility than others, and V_2ZnB has the lowest deformation resistance. The *Y* value denotes the stiffness of solids and is closely related to thermal shock resistance (inverse relation) and melting temperature (direct relation). Based on the *Y* values, the phases can be ranked as follows: $V_2PB > V_2GeB > V_2TlB >$. Thus, V_2PB is expected to be stiffest, and V_2ZnB exhibits the highest thermal shock resistance. Although these three moduli do not directly measure hardness, they tend to be higher for harder solids. As seen in Table 4, the highest value of elastic constants and moduli is observed for V_2PB. Thus, V_2PB is expected to be the hardest among the titled borides, reflected by the Vickers hardness shown in Table 5.

MAX phases usually have higher elastic moduli due to their pre-

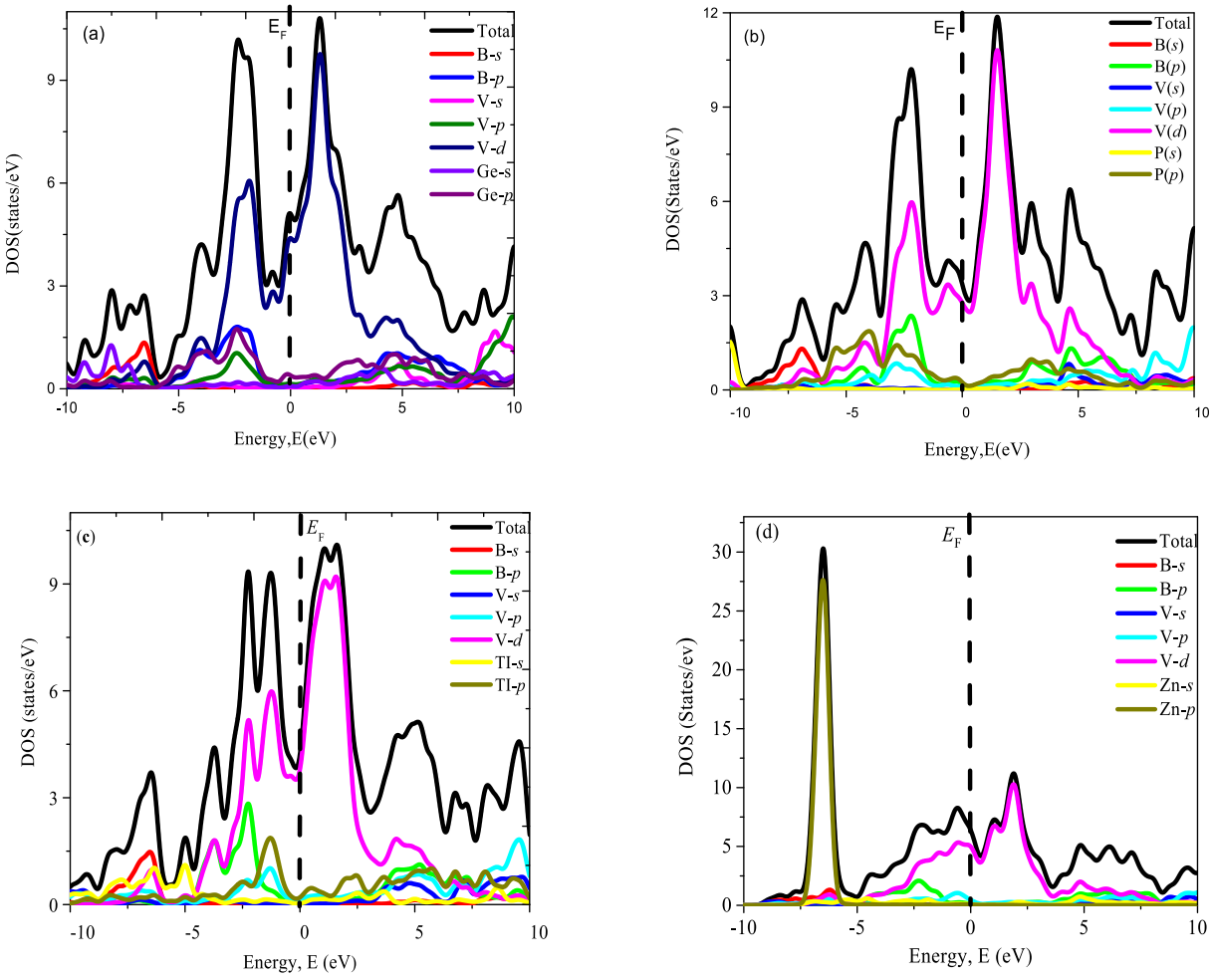

Fig. 4. The total and partial DOS of (a) V_2GeB, (b) V_2PB, (c) V_2TlB, and (d) V_2ZnB borides.

Table 3
Mulliken (atomic) population analysis of V_2AB [A = Ge, P, Tl, Zn] borides.

Phase	Atoms	S	P	d	Total	Charge
V_2GeB	B	1.14	2.45	0.00	3.59	−0.59
	V	2.27	6.74	3.86	12.88	0.12
	Ge	1.11	2.55	0.00	3.66	0.34
V_2PB	B	1.15	2.39	0.00	3.54	−0.54
	V	2.20	6.65	3.92	12.77	0.23
	P	1.57	3.34	0.00	4.91	0.09
V_2TlB	B	1.14	2.52	0.00	3.66	−0.66
	V	2.21	6.70	3.79	12.70	0.30
	Tl	1.10	1.82	10.02	12.94	0.06
V_2ZnB	B	1.13	2.50	0.00	3.63.	−0.63
	V	2.19	6.76	3.75	12.70	0.30
	Zn	0.62	1.14	9.94	11.96	0.04

dominant covalent bonding despite being metallic in nature. This covalent bonding also contributes to the brittleness of most MAX phases, although some can also be ductile. A material's ductile/brittleness character can be studied using two well-known parameters: Pugh [65] and Poisson's [66] ratio. The Pugh ratio is the ratio of shear to bulk moduli (G/B) or bulk to shear moduli (B/G). A material is considered brittle if G/B is higher than 0.57 and ductile if it is lower than 0.57. For Poisson's ratio (ν), a material is considered brittle when the value is lower than 0.26 and ductile if it is higher than 0.26. As shown in Table 4, V_2GeB and V_2ZnB have G/B values lower than 0.571 and ν values higher than 0.26, indicating their ductile nature. On the other hand, V_2PB and V_2TlB have G/B values higher than 0.571 and ν values lower than 0.26, indicating their brittle nature. V_2GeC is also ductile, while V_2ZnC is not ductile. Some Nb-based carbides (Nb_2TlC, Nb_2ZnC, and Nb_2CdC) are also reported as ductile [67]. In addition, Poisson's ratio also carries significant information when classifying the solids into ductile or brittle classes. For instance, the value of ν distinguishes the dominating role of central or non-central interatomic forces within the solids [68]. A value of ν between 0.25 and 0.50 suggests the effectiveness of the central forces inside the solid. In contrast, a value of ν outside this range suggests the dominance of non-central interatomic forces within the solids. It is seen from Table 4 that the non-central interatomic forces dominate the V_2PB and V_2TlB solids. On the other hand, V_2GeB and V_2ZnB are predominantly governed by the central interatomic forces. Furthermore, the dominating bonding character is defined by the ν value; ν is typically 0.1 or less for covalently bonded solids, while it is 0.33 or greater for ionic solids bonds [69]. For brittle MAX phases, ν lies toward the critical value of 0.26, and for ductile phases, it is <0.33, indicating the existence of both covalent and ionic bonding within them.

The machinability index is a crucial parameter that indicates how easily a material can be machined in any form. The ratio of the material's bulk modulus (B) to the shear elastic constant (C44) is known as the machinability index, $\mu = B/C_{44}$, formulated by Sun et al. [70]. In Table 4, it can be observed that the μ values of the titled borides are closer to those of 211 counterpart carbides. Notably, V_2ZnB exhibits the highest value (1.79) of μ, which is also higher than its carbide counterpart ($V_2ZnC \sim 1.49$). As per the equation mentioned above, the value of μ is inversely related to the shear elastic constant C_{44}. Among the herein-studied borides, V_2PB exhibits the lowest μ value with the highest

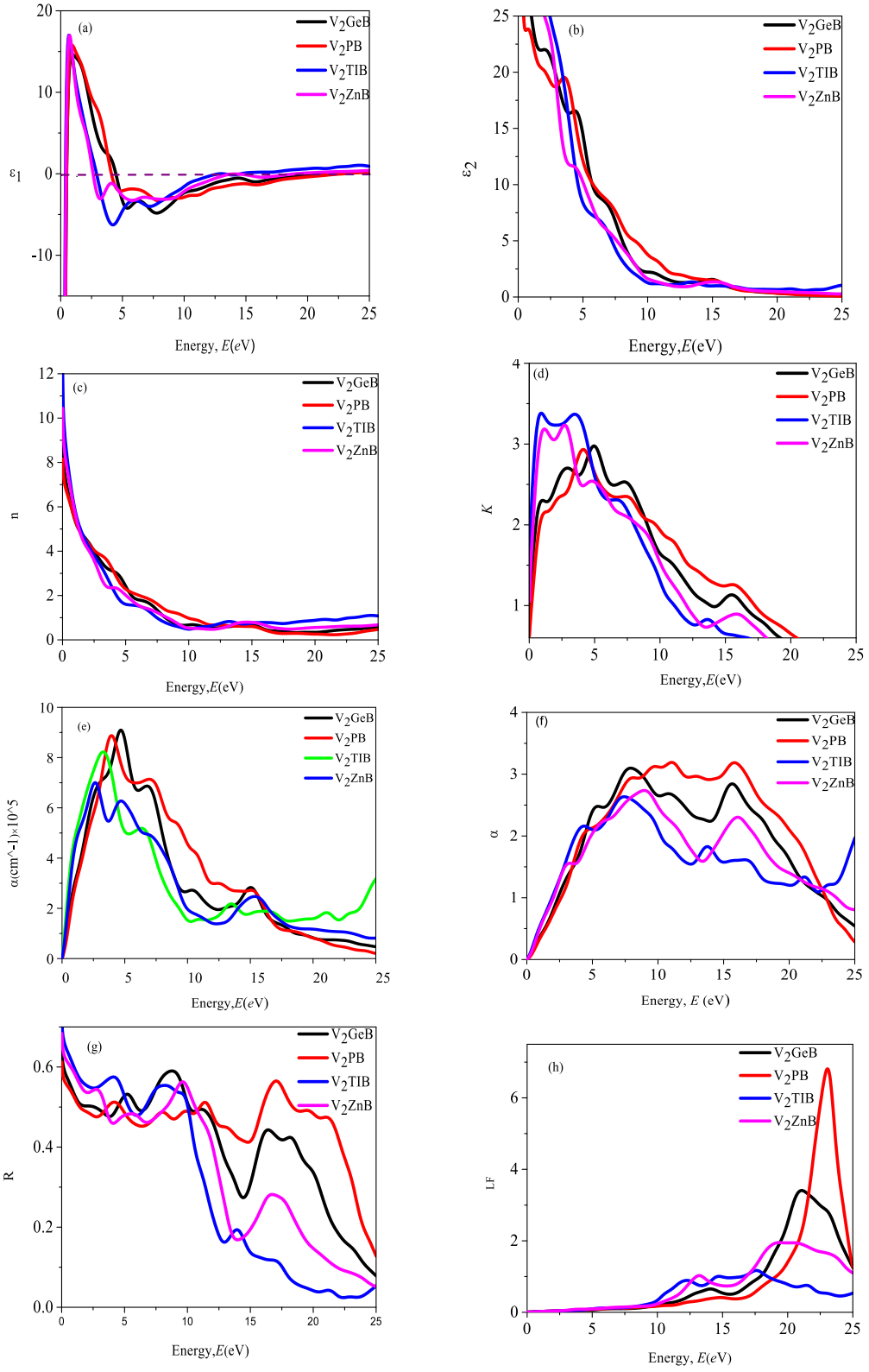

Fig. 5. The charge density mapping of V_2AB [A = Ge, P, Tl, Zn] borides.

value of C_{44}. Similar reports are also available. For example, the highest machinability score of 33.33 is reported for W_2SnC, with a small C_{44} value of 6 GPa, the lowest among all the 211 MAX phases [71]. Among the 312 MAX phases, Ti_3InC_2 has the highest B/C_{44} ratio, with a C_{44} value of 92 GPa [72].

The ability of a solid material to withstand plastic deformation, dents, and scratches is a measure of its hardness [50]. This mechanical property plays a crucial role in determining the suitability of materials for a wide range of engineering applications [73]. The calculation/measurement of hardness depends significantly on the formalisms/methods used, and the results obtained vary broadly. In this paper, we calculated the Vickers hardness of the studied phases using the following

Table 4
Calculated stiffness constants, bulk modulus (B), machinability index (B/C_{44}), Cauchy pressure (CP), shear modulus (G), Young's modulus(ν), and Pugh ratio (G/B) of V_2AB [A = Ge, P, Tl, Zn] borides.

Phase	C_{11} (GPa)	C_{12} (GPa)	C_{13} (GPa)	C_{33} (GPa)	C_{44} (GPa)	B (GPa)	G (GPa)	Y (GPa)	ν	G/B	B/C_{44}	Ref.
V_2GeB	254	119	155	251	162	179	88	227	0.29	0.49	1.11	
[a]V_2GeC	282	121	144	259	160	182	99	252	0.27	0.55	1.13	[61]
V_2PB	343	116	149	365	215	208	143	349	0.22	0.69	0.97	
[b]V_2PC	376	113	168	386	204	226	154	376	0.22	0.68	1.10	[62]
V_2TlB	230	55	62	208	77	114	80	195	0.22	0.70	1.48	
[c]Ti_2TlC	274	73	51	241	82	126	93	224	0.20	0.74	1.53	[63]
V_2ZnB	230	89	82	199	72	129	69	176	0.27	0.53	1.79	
[d]V_2ZnC	308	90	92	260	106	158	104	256	0.22	0.69	1.49	[64]

[a] [61].
[b] [62].
[c] [63].
[d] [64].

Table 5
The Mulliken bond number (n^μ), bond length (d^μ), bond overlap population (p^μ) of μ type, metallic population (P^μ), bond volume (V_b^μ), and Vickers hardness (H_v) of V_2AB [A = Ge, P, Tl, Zn] borides.

Compound	Bond	n^μ	d^μ (Å)	P^μ	$P^{\mu'}$	V_b^μ(A^3)	H_v (GPa)
V_2GeB	B-V	4	2.10	1.13	0.026	24.64	3.91
V_2PB	B-V	4	2.13	1.00	0.298	9.55	12.05
	P-V	4	2.39	0.93	0.298	13.49	
V_2TlB	B-V	4	2.09	0.98	0.115	29.44	2.27
V_2ZnB	B-V	4	2.07	1.00	0.098	25.36	3.04

formalism. Gao [74] anticipated a model to theoretically determine the Vickers Hardness of nonmetallic compounds, which is eventually ineffective in the case of compounds where partial metallic bonds, such as MAX phase compounds, are present [75]. Gou et al. [75] overcome this limitation by introducing the term "metallic populations" into the equation as follows:

$$H_v^\mu = 740(P^\mu - P^{\mu'})\left(v_b^\mu\right)^{(-5/3)}$$

where P^μ is the Mulliken overlap population of the μ-type bond. The $P^{\mu'} = n_{free}/V$, is the metallic population. $n_{free} = \int_{E_P}^{E_F} N(E)dE$ is the total number of free electrons in a cell and V is the unit cell volume. E_P represents the energy at pseudogap. The volume of a bond of the μ-type, v_b^μ, is determined by the bond length d^μ of the μ-type and the number of bonds N_b^ν of type ν per unit volume, given by the equation $v_b^\mu = (d^\mu)^3/\sum_\nu\left[(d^\mu)^3 N_b^\nu\right]$. Finally, the geometric average of all the bonds hardnesses (more than one) present within the solids can be obtained by the following equation [76]: $H_V = \left[\Pi^\mu\left(H_v^\mu\right)^{n^\mu}\right]^{1/\sum n^\mu}$ where, n^μ is the number of bonds of μ-type comprising the actual multiband crystal. In Table 5, the hardness values of the compounds are listed as follows: $V_2PB > V_2GeB > V_2ZnB > V_2TlB$, according to the prediction made in the previous section. In addition, the H_v values for V_2GeB, V_2ZnB, and V_2TlB are within the range of 2–8 GPa [67], indicating the softness and easy machinability of the studied MAX phases, while the *Hv* of V_2PB is much higher than those of V_2GeB, V_2ZnB, and V_2TlB. P-based MAX phases usually exhibit higher hardness values due to the presence of two strong covalent bonds, M-B and P—B bonding [Table 5]; on the other hand, there is only one covalent bonding among M and B atoms for V_2GeB, V_2ZnB, and V_2TlB phases [Table 5]. A similar report is also available for other P-based MAX phases, for example, Nb_2PC (9.3 GPa) and Nb_2GeC (1.49 GPa), Nb_2TlC (1.99 GPa), and Nb_2ZnC (2.29 GPa) [67]. The elastic moduli of V_2PB are also highest, followed by V_2GeB. The bulk modulus also follows the same trend ($V_2PB > V_2GeB > V_2ZnB > V_2TlB$) as H_v, whereas the *G* and *Y* values are higher for V_2TlB than those of V_2ZnB. Additionally, V_2PB has much higher elastic moduli and Vickers hardness compared to the other three compounds, as expected from the charge density mapping.

3.3.1. Elastic anisotropy

The study of the elastic anisotropy of hexagonal layered structured solids is important due to the difference in the atomic arrangement and bonding strength in the c-direction and a(b) -direction. Anisotropy has a crucial connection with several physical phenomena, such as crack formation and propagation, phase changes, dislocation dynamics, precipitation, anisotropic deformation due to plasticity, mechanical yield points, fracture behavior, material friction, and elastic instability. The knowledge of elastic anisotropy also helps in understanding the elastic response under the application of forces. Different anisotropy parameters are being used for different crystal systems. The V_2AB (A = Ge, P, Tl, Zn) MAX phases belong to the hexagonal materials. Thus, we have considered the anisotropic indices that are relevant to hexagonal systems and studied the anisotropic nature of the elastic properties of V_2AB (A = Ge, P, Tl, Zn) borides.

First of all, we considered the shear anisotropic factors that offer invaluable insights into the anisotropy in atomic bonding along the different directions, providing a greater understanding of their practical applications. The formulae used to derived them are as follows: $A_1 = \frac{1/6\,(C_{11}+C_{12}+2C_{33}-4C_{13})}{C_{44}}$, $A_2 = \frac{2C_{44}}{C_{11}-C_{12}}$, $A_3 = A_1.A_2 = \frac{1/3\,(C_{11}+C_{12}+2C_{33}-4C_{13})}{C_{11}-C_{12}}$ [77] for {100} planes between the ⟨011⟩ and ⟨010⟩ directions, for {010} shear planes between the ⟨101⟩ and ⟨001⟩ directions and for {001} shear planes between the ⟨110⟩ and ⟨010⟩ directions, respectively. The results presented in Table 6 reveal that the titled borides exhibit different A_i values, indicating anisotropic behavior in three shear planes. Additionally, the distinct A_1, A_2, and A_3 values highlight the substantial directional dependence of shear modulus in these boride phases.

We have also calculated the ratio of linear compressibility (k_c/k_a) along the *c* and *a*-axes by the following equation:

$$\frac{k_c}{k_a} = \frac{C_{11}+C_{12}-2C_{13}}{C_{33}-C_{13}}$$

From Table 6, the ratio of k_c to k_a is not equal to one for the borides studied herein, indicating an unequal compressibility in the *c* and *a* direction. A k_c/k_a value greater than one suggests a greater compressibility along the *c* direction, while a greater compressibility along the *a*

Table 6
Calculated data for different anisotropy parameters A_1, A_2, A_3, k_c/k_a, A_B, A_G, and the universal anisotropy index (A^U) of V_2AB (A = Ge, P, Tl, Zn) borides.

Phases	A_1	A_2	A_3	k_c/k_a	A_B	A_G	A^U
V_2GeB	0.26	2.40	0.63	0.66	0.2	0.136	1.58
V_2PB	0.46	1.89	0.87	0.75	0.2	0.059	0.63
V_2TlB	0.98	0.88	0.86	1.10	0.0	0.006	0.06
V_2ZnB	0.90	1.02	0.92	1.29	0.3	0.007	0.08

direction is confirmed by a value less than one. Thus, the compressibility is greater along the *c*-direction for V_2TlB and V_2ZnB and reverse for V_2GeB and V_2PB.

After that, we look forward to the percentage anisotropy, which is calculated by the following formulae: $\boldsymbol{A_B} = \frac{B_V - B_R}{B_V + B_R} \times \mathbf{100}\%; \boldsymbol{A_G} = \frac{G_V - G_R}{G_V + G_R} \times \mathbf{100}\%$.

A_B and A_G represent the percentage anisotropy in bulk and shear modulus, respectively. The subscripts V (Voigt) and R (Reuss) represent the upper and lower values of *B* and *G*. A zero (non-zero) value of A_B and A_G indicates the isotropy (anisotropy) in *B* and *G*, where the deviation from zero measures the degree of anisotropy. Table 6 lists the values of A_B and A_G, which indicate the presence of anisotropy in *B* and *G*.

Finally, the universal anisotropy constant, A^U, has also been calculated for the titled borides. The A^U also provides a quantitative measurement of the anisotropy, like A_B and A_G, providing the level of anisotropy possessed by the elastic parameters of the solids, and the following formula has been used for the purpose mentioned above [15]:

$$A^U = 5\frac{G_V}{G_R} + \frac{B_V}{B_R} - 6 \geq 0$$

Upon examining Table 6, it is evident that the value of A^U is non-zero for each phase considered, signifying that V_2AB (A = Ge, P, Tl, Zn) borides display anisotropic characteristics, that is, the parameters used to characterize the mechanical behavior are dependent on the direction measured.

In the end, the nature and extent of the anisotropy of mechanical properties are crucial for practical applications. For example, the materials can behave differently under loading in different directions; the materials could be stiffer or weaker in certain directions. This knowledge of anisotropy is important for different industries, including aerospace, automotive, and material engineering, as it impacts the design of structures. Therefore, the anisotropic indices presented in Table 6 indicate that priority should be given to direction-dependent properties before using these borides.

3.4. Thermal properties

The thermal properties characterizing parameters must be known to evaluate the material's performance and application in a high-temperature environment. In this section, we have investigated the thermal properties to disclose the possible application of the herein-predicted compounds in high-temperature technology. Recently, the MAX phases have drawn significant attention for their application as TBC materials [78,79]. We have considered the Debye temperature (Θ_D), phonon thermal conductivity (k_{ph}), minimum thermal conductivity (k_{min}), thermal expansion coefficient (TEC), and melting temperature (T_m) of the tiled borides in this study because of their significant roles in designing thermal barrier coating materials. For instance, the Debye temperature helps to disclose the behavior of phonons in materials. In contrast, the phonon thermal conductivity and minimum thermal conductivity are important for determining the heat transport properties. The thermal expansion coefficient measures the material's response to changes in temperature, and the melting temperature indicates the material's stability at elevated temperatures. Overall, these parameters are essential for predicting and optimizing the thermal barrier properties of coating materials. Table 7 lists the results obtained for V_2AB (A = Ge, P, TI, Zn) MAX phase borides and those of corresponding counterpart carbides. The Debye temperature has been calculated using the widely known Anderson formula [80,81] based on the sound velocity propagating through the solids. The relevant equations are given below:

$$\boldsymbol{\Theta_D} = \frac{h}{k_B}\left[\left(\frac{3n}{4\pi}\right)\frac{N_A\rho}{M}\right]^{\frac{1}{3}}\boldsymbol{v_m}$$

where,

$$\boldsymbol{v_m} = \left[\frac{1}{3}\left(\frac{1}{{v_l}^3} + \frac{2}{{v_t}^3}\right)\right]^{-\frac{1}{3}}$$

with,

$\boldsymbol{v_l} = \left(\frac{3B+4G}{3\rho}\right)^{\frac{1}{2}}$ and $\boldsymbol{v_t} = \left(\frac{G}{\rho}\right)^{\frac{1}{2}}$where, $\boldsymbol{v_m}$ is the average sound velocity, which is computed from the longitudinal ($\boldsymbol{v_l}$) and transverse ($\boldsymbol{v_t}$) sound velocities, respectively, $\boldsymbol{\rho}$ is the mass density, $\boldsymbol{N_A}$ is Avogadro's number, *M* is the molar mass, *n* is the number of atoms in the unit cell, $\boldsymbol{k_B}$ is the Boltzmann's constant and $\boldsymbol{h}$ is the Planck's constant. The $\boldsymbol{v_l}$ and $\boldsymbol{v_t}$ have been computed from the bulk and shear modulus. The obtained Θ_D of the titled compounds is presented in Table 7. The Debye temperature indicates the characteristics of the temperature of solids, which usually describes the vibrational mode of atoms; the higher the Θ_D, the stronger the interatomic bonding. On the other hand, the hardness of solids is determined by the bonding strength of atoms within the solids. Hence, a direct relationship between Debye temperature and hardness is expected, and a higher Θ_D is also expected for harder solids [60]. Tables 5 and 7 show that higher Θ_D is obtained for harder phases studied herein. The Θ_D is also comparable to other MAX phases [82,83].

The lattice thermal conductivity of solids is a decisive property for applications at elevated temperatures, specially, at very high temperatures, when the thermal conductivity becomes constant and known as minimum thermal conductivity. Thus, the study of thermal conductivity is essential, and we have also calculated the thermal conductivity and minimum thermal conductivity of the titled solids, which are presented in Table 7. The relevant formulae are given below:

[84]:

$$\boldsymbol{k_{ph}} = \boldsymbol{A}(\gamma)\frac{\boldsymbol{M_{av}}{\boldsymbol{\Theta_D}}^3\boldsymbol{\delta}}{\boldsymbol{\gamma^2 n^{\frac{2}{3}} T}}$$

where $\boldsymbol{\gamma} = \frac{3(1+\upsilon)}{2(2-3\upsilon)}$ and $\boldsymbol{A}(\gamma) = \frac{4.85628\times10^7}{2\left(1-\frac{0.514}{\gamma}+\frac{0.228}{\gamma^2}\right)}$

The lattice thermal conductivity of the studied MAX phases is 30.7, 82.8, 27.0, and 17.2 W/mK for V_2GeB, V_2PB, V_2TlB, and V_2ZnB, respectively. At room temperature, MAX phase compounds generally exhibit total thermal conductivity values ranging from 12 to 60 W/mK [2]. As seen, the K_{ph} of V_2PB falls outside the range mentioned above. A higher value of thermal conductivity (65 W/mK) was reported for 212

Table 7
The Debye temperature (Θ_D), phonon thermal conductivity (k_{ph}), minimum thermal conductivity (k_{min}), thermal expansion coefficient (TEC), and melting temperature (T_m) of V_2AB (A = Ge, P, TI, Zn) borides.

Phases	ρ (kg/m^3)	υ_l (m/s)	υ_t (m/s)	υ_m (m/s)	Θ_D (K)	γ	k_{ph} (W/mK)	k_{min} (W/mK)	*TEC* (K^{-1} × 10^{-6})	T_m (K)	*Ref.*
V_2GeB	6243.1	7084.4	4002.2	4451.4	573.8	1.54	30.7	1.10	3.6	1492	This
V2GeC	6670.0	6864.0	3858.0	4293.0	565.0	1.32	39.9	1.10		1588	[54
V_2PB	5174.8	8904.7	5401.8	5969.2	786.9	1.32	82.8	1.54	2.6	1930	This
V2PC	3441.0	11,196.0	6689.8	7403.6	849.5	1.36	97.8	1.45		2061	[62]
V_2TlB	8941.1	4982.9	3009.9	3327.4	404.3	1.32	27.0	0.73	4.1	1356	This
Ti_2TlC	8454.1	5437.9	3316.7	3663.1	439.1	1.14	27.0	0.78		1537	[63]
V_2ZnB	5828.3	6157.8	6157.8	3830.4	489.1	1.60	17.2	0.93	5.3	1342	This
V_2ZnC	6166.0	6940	4110.0	4550.0	592.0	1.32	44.6	1.14		1482	[64]

MAX phase borides (Nb_2PB_2) [85]. In their work, the authors highlighted the critical role of high thermal conductivity in thin films. They stressed that such films are extensively utilized in the microelectronic packaging industry as protective layers or support materials, where a high level of conductivity is necessary. Thus, the thin film of V_2PB is likely to be suitable for use as supporting materials for the same mentioned earlier.

The minimum thermal conductivity (k_{min}) was calculated via the equation given below [86]:

$$k_{min} = k_B v_m \left(\frac{M}{\eta \rho N_A}\right)^{-\frac{2}{3}}$$

Before addressing the minimum thermal conductivity, let's start by discussing the k_{min} values of well-known TBC materials used in gas turbines, airplanes, and cutting-edge aero engines. Yttria-stabilized zirconia (7YSZ) with a k_{min} of 2.20 W/mK has been extensively used as a TBC material, providing valuable insights to researchers [87]. Researchers have also explored other TBC materials with high T_m and low thermal conductivity. The rare-earth-based oxides, $RE_2T_2O_7$ (RE = La, Pr, Nd, Sm, Eu, Gd, Y, Er, or Lu and T = Ti, Mo, Sn, Zr, or Pb) with k_{min} values ranging from 1.40 to 3.05 W/mK, have been discovered [87,88]. The rare earth stannates $RE_2Sn_2O_7$ (RE = La, Nd, Sm, Gd, Er, and Yb) have a k_{min} range from 1.80 to 2.50 W/mK [87]. Some of the perovskite oxides, also known as TBC materials, are ABO_3 (A = Sr, Ba; B = Ti, Zr, Hf), which have k_{min} values in the range of 1.09 to 1.74 W/mK [87]. As seen in Table 7, the highest k_{min} (1.54 W/mK) is found for V_2PB, which is lower than that of many other TBC materials. Thus, the titled compounds are expected to be potential TBC materials.

The thermal expansion coefficient (*TEC*) is another critical parameter that need to be known before using a material in high-temperature environment to prevent the structure getting damaged due to thermal stress developed during operation at high temperatures. The *TEC* of the titled compounds was calculated by the following equation[89]:

$$\mathbf{TEC} = \frac{\gamma C_v}{3 B_T V_m}$$

where γ = Grüneisen parameter, C_v = specific heat at constant volume, B_T = isothermal bulk modulus, and V_m = molar volume.

The TEC values are comparable (in the order of 10^{-6} K^{-1}) to those of a thermally grown oxide layer in extreme conditions, a prerequisite for TBC materials at very high temperatures. Thus, the studied phases are expected to be potential materials for high-temperature applications.

Finally, the melting temperatures of the V_2AB (A = Ge, P, TI, Zn) MAX phases are also calculated using the equation given below [16].

$$T_m = 354 + 1.5(2C_{11} + C_{33}).$$

As seen, the equation contains C_{11} **and** C_{33} with conversion parameter. Thus, a direct relationship of T_m with Young's modulus (Young's modulus is the measure of stiffness of solids, and C_{11} and C_{33} are the measure of stiffness along the x and z-direction of solids) is expected. The data presented in Table 4 and Table 7 confirmed this relationship. The T_m is high enough (above 1000 °C), and the TBC is usually used to protect the heating elements in the hottest parts of different engines.

Based on the parameters used to characterize the materials, such as its machinability index, which indicates the need for good machinability to create a coating layer, minimum thermal conductivity, very low thermal expansion coefficient, and high melting temperature, it can be concluded that the compounds under study are excellent potential materials for TBC applications. In addition, Table 7 revealed that the titled borides can be considered as an alternative to those of carbide phases. In comparison, the Debye and melting temperatures, lattice thermal conductivity, and minimum thermal conductivity of the borides (with an exception for Nb_2SB/Nb_2SC [11], V_2GeB/V_2GeC [Table 6]) are usually lower than those of counterpart carbides [11,15]. Higher Θ_D and T_m are desirable for high-temperature applications, and lower lattice thermal and minimum thermal conductivity are good for thermal barrier coating applications. Thus, the selection of materials depends on the targeted environments, such as operating temperature, and the type of applications, such as TBC applications. In particular, V_2PB exhibits the best combination of thermo-mechanical properties, which might be a possible new material to replace Ni/Co superalloys in the hottest section of a gas turbine engine. This substitution would allow the engine to operate at higher temperatures, potentially boosting efficiency. Currently, Ni/Co superalloys can withstand temperatures of around 1100 °C–1150 °C, but this could possibly be increased by approximately 100 °C using MAX phases. [78]. In order to validate the potential of V_2PB, it is imperative to conduct experimental synthesis and measurements of mechanical properties, melting temperature, minimum thermal conductivity, and coefficient of thermal expansion. Regrettably, these crucial procedures currently fall outside the scope of our present capabilities.

3.5. Optical properties

It is necessary to disclose the material's response to electromagnetic radiation (photons) for the exploration of the practical applications of solids. MAX phase materials are well known as coating materials on spaceships to avoid solar heating of the body, which can be predicted by studying optical properties [90]. By examining the reflectivity of these materials, we can gain insight into their ability to efficiently reflect solar radiation. This understanding allows for the development of coatings with high reflectivity, which can effectively manage solar radiation and minimize heat absorption, thereby reducing the impact of solar heating on the spacecraft. That is why the optical properties of the titled MAX phases have been studied and presented in this section. Before delving into the optical functions, it is imperative to understand the real and imaginary components of the frequency- and energy-dependent dielectric function. Any homogeneous material at any photon energy may have its optical functions described using the dielectric function. The title compounds' electronic structure demonstrated that they were a metallic system, requiring the use of an additional parameter (plasma frequency, 3 eV) in order to analyze the optical properties. Using the momentum matrix element between the occupied and unoccupied electronic states, the imaginary component of the dielectric function (IDF) $\varepsilon_2(\omega)$ has been estimated using the following formula:

$$\varepsilon_2(\omega) = \frac{2e^2\pi}{\Omega \in_0} \sum_{k,\nu,c} |\psi_k^c | u.r | \psi_k^\nu |^2 \delta\left(E_k^c - E_k^\nu - E\right)$$

where, e = electronic charge; ω = light frequency; u = polarizing vector of incident electric field; ψ_k^c = conduction band wave function at k and ψ_k^v = valence band wave function at k. The real part of the dielectric function (RDF) [$\varepsilon_1(\omega)$] was computed using the Kramers-Kronig relations [27,91].

$$\varepsilon_1(\omega) = 1 + \frac{2}{\pi} P \int_0^\infty \frac{\omega' \varepsilon_2(\omega') d\omega'}{(\omega'^2 - \omega^2)}$$

After that, the refractive index η(ω), the extinction coefficient $k(\omega)$, the absorption coefficient α(ω), the photoconductivity σ(ω), reflectivity R (ω), and the energy loss function L(ω) were calculated using the following equations:

$$n(\omega) = \frac{1}{\sqrt{2}} \left[\sqrt{\{\varepsilon_1(\omega)\}^2 + \{\varepsilon_2(\omega)\}^2} + \varepsilon_1(\omega) \right]^{1/2}$$

$$k(\omega) = \frac{1}{\sqrt{2}} \left[\sqrt{\{\varepsilon_1(\omega)\}^2 + \{\varepsilon_2(\omega)\}^2} - \varepsilon_1(\omega) \right]^{1/2}$$

$$\alpha(\omega) = \sqrt{2}\omega \left[\sqrt{\{\varepsilon_1(\omega)\}^2 + \{\varepsilon_2(\omega)\}^2} - \varepsilon_1(\omega) \right]^{1/2}$$

$$\sigma(\omega) = \frac{\omega\varepsilon_2}{4\pi}$$

$$R(\omega) = \left| \frac{\sqrt{\varepsilon(\omega)} - 1}{\sqrt{\varepsilon(\omega)} + 1} \right|^2$$

$$L(\omega) = \varepsilon_2(\omega) \Big/ \left[\{\varepsilon_1(\omega)\}^2 + \{\varepsilon_2(\omega)\}^2 \right]$$

Therefore, this section presents a thorough investigation of the energy-dependent (0 to 25 eV) optical constants of V_2AB (A═Ge, P, TI, Zn) MAX phase borides.

The dielectric function is made up of two parts: the IDF [$\varepsilon_2(\omega)$] and the RDF [$\varepsilon_1(\omega)$], as shown in Fig. 6(a, b), where $\varepsilon_2(\omega)$ is connected to dielectric losses as a function of frequency and $\varepsilon_1(\omega)$ represents stored energy. The energy-dependent $\varepsilon_1(\omega)$ spectra start from below and reach zero at approximately 20 eV, as seen in Fig. 6(a-b). In contrast, the $\varepsilon_2(\omega)$ value approaches zero from above about 23 eV, providing evidence for metallic or Drude-like behavior. The low-energy region (< 1 eV) of the $\varepsilon_1(\omega)$ spectra exhibits the highest dielectric constant value due to the electron's transition within the bands. The infrared spectrum of $\varepsilon_2(\omega)$ gradually declined with a prominent peak at 3 eV. The compounds under examination exhibit almost same RDF and IDF spectra.

The extinction coefficient (k) shows how much light a material absorbs, whereas the refractive index (n) compares the velocity of light in any medium with that in empty space. The refractive index (n) and extinction coefficient (k) of V_2AB (A = Ge, P, TI, Zn) phases are shown in Fig. 6 (c, d). At zero photon energy/frequency, the V_2AB (A = Ge, P, TI, Zn) MAX phases exhibit n values of 9, 8, 12, and 10.5 values, respectively. For photonic and optoelectronic device applications, materials having a high refractive index (often >1.5) are beneficial for improving the visual quality of electronic displays such as QDLED TVs, OLEDs, and LCDs [91–93]. V_2TlB has the highest n value (12) out of all the compounds, whereas V_2PB has the lowest n value (8).

We have also calculated the absorption spectra of V_2AB (A = Ge, P, TI, Zn) borides, as shown in Fig. 6(e). The spectra started at zero photon energy, revealing their metallic character. The spectra grow fast in the visible light region and reach their maximum in the ultraviolet region, which then decreases progressively. The materials above demonstrate a broad absorption spectrum, or absorption capability, predominantly in the visible and ultraviolet wavelength ranges. This implies they may find application in developing diverse optoelectronic devices, including UV surface-disinfection apparatus and medical sterilization devices. These materials' photoconductivity behavior closely matches their absorption characteristics, as seen in Fig. 6(f). They also begin with the starting of incident photon, which agrees well with their band structure results. The compounds' conductivity peaked at around 5 eV energy and gradually decreased with few visible peaks. Interestingly, the visible region finds one prominent peak at around 2.5 eV. However, a closer look at the electrical structure lends credence to the claim that these results strongly suggest that the materials in question shouldn't have a band gap.

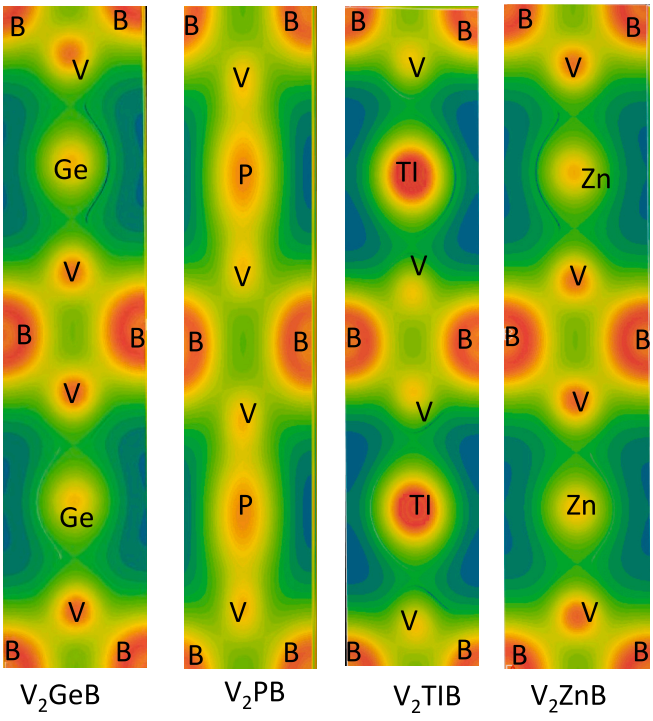

Fig. 6. The (a) real and (b) imaginary part of the dielectric function, (c) absorption coefficient, (d) photoconductivity, (e) refractive index, (f) extinction coefficient, (g) reflectivity, and (h) loss function of V_2AB (A = Ge, P, TI, Zn) borides.

The quantity of light energy a surface reflects before absorbing is known as its reflectivity (Fig. 6(g)). The initial reflectivity spectra of the V_2GeB, V_2PB, V_2TlB, and V_2ZnB are 65, 62, 70, and 68 %, respectively. This spectrum shows values in the visible and infrared areas that are consistently above 47 %. The reflectivity graphs show a prominent peak at around 8 eV, after which the reflectivity of the substances under investigation drops rapidly as photon energy increases. According to reports [90,94], solar light may be successfully reflected from the surface of materials if it has an average reflectivity of 44 % or greater. As evident from Fig. 6 (g), the reflectivity of the studied phases sustained higher values (higher than 44 %) up to the UV–Vis range, which indicates that they can reflect solar radiation from their surface. Thus, spaceships can be protected from solar heating by making a surface coating of these MAX phases.

The energy dissipated during the passage of charged particles across a medium, like electrons. It is clear from Fig. 6 (h) that there is no energy loss up to 0–10 eV for all the compounds under study because of the comparatively large value of [$\varepsilon_2(\omega)$]. At the point of maximal energy loss, we find a plasma resonance. The energy loss of the charged particle is expressed by prominent peaks for V_2GeB, V_2PB, V_2TlB, and V_2ZnB, which were found at 20.5, 22, 17.5, and 20 eV, respectively. The compounds that are being studied should have high transmittance; the absorption and reflection spectra should show abrupt decreases at these particular energies.

4. Conclusions

The MAX phase borides V_2AB [A = Ge, P, Tl, Zn] have been explored for the first time. The formation energy confirmed their chemical stability, the phonon dispersion curve confirmed their dynamical stability and elastic constants confirmed their mechanical stability. The overlapping of valence and conduction bands at the Fermi level reveal the metallic behavior of V_2AB [A = Ge, P, Tl, Zn] borides. The DOS displays a finite value at E_F with a dominating contribution from the V-*d* states. The hybridization of different states suggests the presence of covalent bonding. In contrast, the Mulliken population confirms the transfer of charges from V and A atoms to B atoms, revealing the formation of ionic bonds. The CDM demonstrates variation in bonding strength, leading to changes of the elastic moduli and Vickers hardness for different phases. The elastic constants and moduli of the studied phases are compared with those counterpart carbides where available. The findings show that borides could serve as an alternative to carbides. V_2GeB and V_2ZnB (V_2PB and V_2TlB) are ductile (brittle) like their carbide phases. Among these, V_2ZnB is more machinable than others. The Vickers hardness values agree with the charge density mapping, showing a much higher value for V_2PB compared to the other three compounds studied. The different anisotropic indices suggest the anisotropic nature of the mechanical properties. The parameters characterizing the thermal properties, such as Θ_D, k_{ph}, k_{min}, *TEC*, and T_m, are comparable to those of conventional MAX phase carbides [22,82,95]. The results also suggest

their potential use in high-temperature technology, such as TBC materials. The optical constants, $\varepsilon_1(\omega)$, $\varepsilon_2(\omega)$, α and σ spectra reveal the metallic nature of the studied phases. The reflectivity of each phase is continuously above the 44 % up to UV range, certifying a good potential for use as coating materials in spaceships as solar heating reflectors, like most of the MAX phase carbides.

Therefore, the herein-explored MAX phase borides have the potential to be an alternative to the well-known carbide MAX phases. The non-existence of previous studies on these borides has resulted in a lack of additional theoretical or experimental data in tables and figures. This study effectively addresses this gap and provides valuable data for future experimental research. We hope that the materials scientists will pay attention to synthesizing these borides experimentally and unlock their full potential for the advancement of the scientific community and the benefit of practical applications.

CRediT authorship contribution statement

M.A. Ali: Writing – original draft, Supervision, Project administration, Methodology, Funding acquisition, Formal analysis, Conceptualization. **S. Nath:** Visualization, Investigation, Formal analysis, Data curation. **S. Mahmud:** Investigation, Formal analysis, Data curation. **N. Jahan:** Writing – review & editing, Validation, Formal analysis. **M.M. Uddin:** Writing – review & editing, Writing – original draft, Validation.

Declaration of competing interest

The authors declare that they have no known competing financial interests or personal relationships that could have appeared to influence the work reported in this paper.

Acknowledgments

This work was carried out in ACMRL, which was established with the aid of a grant (grant number: 21-378 RG/PHYS/AS_G -FR3240319526) from UNESCO-TWAS and the Swedish International Development Cooperation Agency (SIDA). The views expressed herein do not necessarily represent those of UNESCO-TWAS, SIDA, or its Board of Governors. M. A. Ali, S. Nath, and N. Jahan are grateful to the UGC, Bangladesh, for providing financial support to carry out this research (Project code: Physical Science: 2022-2023/44).

Data availability

Data will be made available on request.

References

[1] M.W. Barsoum, T. El-Raghy, Synthesis and characterization of a remarkable ceramic: Ti3SiC2, J. Am. Ceram. Soc. 79 (1996) 1953–1956, https://doi.org/10.1111/j.1151-2916.1996.tb08018.x.
[2] M.W. Barsoum, MAX Phases: Properties of Machinable Ternary Carbides and Nitrides, Wiley-VCH Verlag GmbH & Co. KGaA, Weinheim, Germany, 2013, https://doi.org/10.1002/9783527654581.
[3] A. Srivastava, M. Radovic, Mechanical properties and microstructure evolution of Ti2AlC under compression in 25-1100°C temperature range, Acta Mater. (2020), https://doi.org/10.1016/j.actamat.2020.02.057.
[4] D. Music, A. Houben, R. Dronskowski, J.M. Schneider, Ab initio study of ductility in M2AlC (M = Ti, V, Cr), Phys. Rev. B 75 (2007) 174102, https://doi.org/10.1103/PhysRevB.75.174102.
[5] M. Dahlqvist, M.W. Barsoum, J. Rosen, MAX phases – past, present, and future, Mater. Today (2023), https://doi.org/10.1016/j.mattod.2023.11.010.
[6] T. Rackl, L. Eisenburger, R. Niklaus, D. Johrendt, Syntheses and physical properties of the MAX phase boride Nb2SB and the solid solutions N b2 S Bx C1-x(x=0-1), Phys. Rev. Mater. 3 (2019) 054001, https://doi.org/10.1103/PhysRevMaterials.3.054001.
[7] T. Rackl, D. Johrendt, The MAX phase borides Zr2SB and Hf2SB, Solid State Sci. 106 (2020) 106316, https://doi.org/10.1016/j.solidstatesciences.2020.106316.
[8] M. Khazaei, M. Arai, T. Sasaki, M. Estili, Y. Sakka, Trends in electronic structures and structural properties of MAX phases: a first-principles study on M 2 AlC (M = Sc, Ti, Cr, Zr, Nb, Mo, Hf, or ta), M 2 AlN, and hypothetical M 2 AlB phases, J. Phys. Condens. Matter 26 (2014) 505503, https://doi.org/10.1088/0953-8984/26/50/505503.
[9] G. Surucu, Investigation of structural, electronic, anisotropic elastic, and lattice dynamical properties of MAX phases borides: An ab-initio study on hypothetical MAB (M = Ti, Zr, Hf; a = Al, Ga, in) compounds, Mater. Chem. Phys. 203 (2018) 106–117, https://doi.org/10.1016/j.matchemphys.2017.09.050.
[10] S. Aydin, A. Tatar, Y.O. Ciftci, Some new members of MAX family including light-elements: Nanolayered Hf2XY (X= Al, Si, P and Y=B, C, N), Solid State Sci. 53 (2016) 44–55, https://doi.org/10.1016/j.solidstatesciences.2015.10.010.
[11] M.A. Ali, M.M. Hossain, M.M. Uddin, M.A. Hossain, A.K.M.A. Islam, S.H. Naqib, Physical properties of new MAX phase borides M2SB (M = Zr, Hf and Nb) in comparison with conventional MAX phase carbides M2SC (M = Zr, Hf and Nb): comprehensive insights, J. Mater. Res. Technol. 11 (2021) 1000–1018, https://doi.org/10.1016/j.jmrt.2021.01.068.
[12] M.S. Hossain, M.A. Ali, M.M. Hossain, M.M. Uddin, Physical properties of predicted MAX phase borides Hf2AB (a = Pb, bi): a DFT insight, Mater. Today Commun. 27 (2021) 102411, https://doi.org/10.1016/j.mtcomm.2021.102411.
[13] M.S. Hossain, N. Jahan, M.M. Hossain, M.M. Uddin, M.A. Ali, High pressure mediated physical properties of Hf2AB (a = Pb, bi) via DFT calculations, Mater. Today Commun. 34 (2023) 105147, https://doi.org/10.1016/j.mtcomm.2022.105147.
[14] S. Sãad Essaoud, A.S. Jbara, Electronic-structural, thermo-electric, and thermo-mechanical properties of M2AC and M2AB (M = Nb or Mo, a = Al or Ga) compounds, Indian J. Phys. 97 (2023) 105–114, https://doi.org/10.1007/s12648-022-02386-0.
[15] M.R. Rana, S. Islam, K. Hoque, G.G. Biswas, M.E. Hossain, S.H. Naqib, M.A. Ali, DFT prediction of the stability and physical properties of M2GaB (M = Sc, V, Nb, ta), J. Mater. Res. Technol. 24 (2023) 7795–7815, https://doi.org/10.1016/j.jmrt.2023.05.008.
[16] S. Islam, M.R. Rana, K. Hoque, G.G. Biswas, M.E. Hossain, M.M. Hossain, M. M. Uddin, S.H. Naqib, M.A. Ali, A comprehensive exploration of the physical properties of M2GaB (M = Ti, Zr, Mo, Hf) through DFT method, Results Mater. 19 (2023) 100438, https://doi.org/10.1016/j.rinma.2023.100438.
[17] Q. Zhang, Y. Zhou, X. San, W. Li, Y. Bao, Q. Feng, S. Grasso, C. Hu, Zr2SeB and Hf2SeB: two new MAB phase compounds with the Cr2AlC-type MAX phase (211 phase) crystal structures, J. Adv. Ceram. 11 (2022) 1764–1776, https://doi.org/10.1007/s40145-022-0646-7.
[18] Q. Zhang, Y. Zhou, X. San, D. Wan, Y. Bao, Q. Feng, S. Grasso, C. Hu, Thermal explosion synthesis of first Te-containing layered ternary Hf2TeB MAX phase, J. Eur. Ceram. Soc. 43 (2023) 173–176, https://doi.org/10.1016/j.jeurceramsoc.2022.09.051.
[19] J. Islam, M.D. Islam, M.A. Ali, H. Akter, A. Hossain, M. Biswas, M.M. Hossain, M. M. Uddin, S.H. Naqib, DFT insights into MAX phase borides Hf 2 AB [a = S, se, Te] in comparison with MAX phase carbides Hf 2 AC [a = S, se, Te], ACS Omega 8 (2023) 32917–32930, https://doi.org/10.1021/acsomega.3c04283.
[20] Y. Zhou, H. Xiang, C. Hu, Extension of MAX phases from ternary carbides and nitrides (X = C and N) to ternary borides (X = B, C, and N): a general guideline, Int. J. Appl. Ceram. Technol. 20 (2023) 803–822, https://doi.org/10.1111/ijac.14223.
[21] X. Bai, K. Chen, K. Luo, N. Qiu, Q. Huang, Q. Han, H. Liang, X. Zhang, C. Bai, Structural, electronic, and mechanical properties of Zr2SeB and Zr2SeN from first-principle investigations, Materials (Basel). 16 (2023) 5455, https://doi.org/10.3390/ma16155455.
[22] R. Akther, N. Jahan, M.A. Ali, Study of New MAX Phase Materials: Sc2AX, A= Bi, Br; X=C, 2024, p. 109679, https://doi.org/10.1016/j.mtcomm.2024.109679. N, B) via Ab-initio Method, Mater. Today Commun.
[23] A.K.M.N. Ishtiaq, M.N. Uddin, N. Afsary, M.K. Alam, S. Islam, M.O.F. Rasel, M. A. Ali, K. Hoque, First-principles study of electronic, mechanical, and optical properties of M3GaB2 (M = Ti, Hf) MAX phases, Heliyon 10 (2024) e33651, https://doi.org/10.1016/j.heliyon.2024.e33651.
[24] P. Hohenberg, W. Kohn, Inhomogeneous electron gas, Phys. Rev. 136 (1964).
[25] W. Kohn, L.J. Sham, Self-consistent equations including exchange and correlation effects, Phys. Rev. 140 (1965) A1133.
[26] S.J. Clark, M.D. Segall, C.J. Pickard, P.J. Hasnip, M.I.J. Probert, K. Refson, M. C. Payne, First principles methods using CASTEP, Zeitschrift Für Krist. - Cryst. Mater. 220 (2005) 567–570, https://doi.org/10.1524/zkri.220.5.567.65075.
[27] M.D. Segall, P.J.D. Lindan, M.J. Probert, C.J. Pickard, P.J. Hasnip, S.J. Clark, M. C. Payne, First-principles simulation: ideas, illustrations and the CASTEP code, J. Phys. Condens. Matter 14 (2002) 2717–2744, https://doi.org/10.1088/0953-8984/14/11/301.
[28] J.P. Perdew, K. Burke, M. Ernzerhof, Generalized gradient approximation made simple, Phys. Rev. Lett. 77 (1996) 3865–3868, https://doi.org/10.1103/PhysRevLett.77.3865.
[29] D. Vanderbilt, Soft self-consistent pseudopotentials in a generalized eigenvalue formalism, Phys. Rev. B 41 (1990) 7892.
[30] T.H. Fischer, J. Almlof, General methods for geometry and wave function optimization, J. Phys. Chem. 96 (1992) 9768–9774, https://doi.org/10.1021/j100203a036.
[31] A. Bouhemadou, R. Khenata, Structural, electronic and elastic properties of M2SC (M=Ti, Zr, Hf) compounds, Phys. Lett. A 372 (2008) 6448–6452, https://doi.org/10.1016/j.physleta.2008.08.066.
[32] X. Wang, K. Chen, E. Wu, Y. Zhang, H. Ding, N. Qiu, Y. Song, S. Du, Z. Chai, Q. Huang, Synthesis and thermal expansion of chalcogenide MAX phase Hf2SeC, J. Eur. Ceram. Soc. 42 (2022) 2084–2088, https://doi.org/10.1016/j.jeurceramsoc.2021.12.062.

[33] M.A. Ali, M.W. Qureshi, DFT insights into the new Hf-based chalcogenide MAX phase Hf2SeC, Vacuum 201 (2022) 111072, https://doi.org/10.1016/j.vacuum.2022.111072.

[34] Q. Fan, C. Liu, J. Yang, First-principles investigations of the structural, elastic, and thermodynamic properties of the MAX phase borides: Hf2AB (a=S, se, and Te), Mater. Today Commun. 37 (2023) 107182, https://doi.org/10.1016/j.mtcomm.2023.107182.

[35] I. Bourachid, D. Rached, H. Rached, A. Bentouaf, Y. Rached, M. Caid, B. Abidri, Magneto-electronic and thermoelectric properties of V-based Heusler in ferrimagnetic phase, Appl. Phys. A 128 (2022) 493, https://doi.org/10.1007/s00339-022-05641-7.

[36] A. Bentouaf, Elastic, half-metallicity, thermodynamic, and transport properties of Ru2VGe and Ru2VSb full-Heusler compounds: a first-principle study, J. Supercond. Nov. Magn. 34 (2021) 157–167, https://doi.org/10.1007/s10948-020-05692-y.

[37] M.W. Qureshi, X. Ma, G. Tang, R. Paudel, Ab initio predictions of structure and physical properties of the Zr2GaC and Hf2GaC MAX- phases under pressure, Sci. Reports 11 (2021) 1–23, https://doi.org/10.1038/s41598-021-82402-1.

[38] Y. Pan, Z. Yang, H. Zhang, Exploring the structural, phonon dynamical, mechanical and thermodynamic properties of TM2AlC(TM=Ti, Zr and Hf) carbides, Diamond Relat. Mater. 144 (2024) 110966, https://doi.org/10.1016/j.diamond.2024.110966.

[39] S. Aydin, 211-MAX borides: the stable boron-substituted 211-MAX compounds by first-principles, Mater. Today Commun. 25 (2020) 101689, https://doi.org/10.1016/j.mtcomm.2020.101689.

[40] M.N. Uddin, A.K..N. Ishtiaq, S. Islam, M.R. Rana, M.A. Ali, K. Hoque, Prediction of new 212 M2AB2 borides as a promising candidate for future engineering: DFT calculations, Mater. Today Commun. (2024) 108536, https://doi.org/10.1016/j.mtcomm.2024.108536.

[41] M. Rougab, A. Gueddouh, First-principles insights into structural stability, elastic anisotropies, mechanical and thermodynamic properties of the Hf2GeX (X=C, N, and B) 211 MAX phases, J. Phys. Chem. Solid 176 (2023) 111251, https://doi.org/10.1016/j.jpcs.2023.111251.

[42] E. Deligoz, H. Ozisik, E. Bolen, Physical insights on the ultralow thermal conductivity of Ag8XSe6 (X = Si, Ge, and Sn), Inorg. Chem. Commun. 142 (2022) 109689, https://doi.org/10.1016/j.inoche.2022.109689.

[43] A.J. Hong, C.L. Yuan, J.-M. Liu, Quaternary compounds ag 2 XYSe 4 (X = Ba, Sr; Y = Sn, Ge) as novel potential thermoelectric materials, J. Phys. D Appl. Phys. 53 (2020) 115302, https://doi.org/10.1088/1361-6463/ab6056.

[44] M.A. Hadi, S.-R. Christopoulos, A. Chroneos, S.H. Naqib, A. Islam, DFT insights into the electronic structure, mechanical behaviour, lattice dynamics and defect processes in the first Sc-based MAX phase Sc2SnC, Sci. Rep. 12 (2022) 1–16.

[45] A. Champagne, F. Bourdarot, P. Bourges, P. Piekarz, D. Pinek, I. Gélard, J.-C. Charlier, T. Ouisse, Phonon dispersion curves in Cr2AlC single-crystals, Mater. Res. Lett. 6 (2018) 378–383.

[46] H. Ozisik, K. Colakoglu, H.B. Ozisik, E. Deligoz, Structural, elastic, and lattice dynamical properties of germanium diiodide (GeI2), Comput. Mater. Sci. 50 (2010) 349–355, https://doi.org/10.1016/j.commatsci.2010.08.026.

[47] M.S. Ali, M.A. Rayhan, M.A. Ali, R. Parvin, A.K.M.A. Islam, New MAX phase compound Mo_2TiAlC_2: first-principles study, J. Sci. Res. 8 (2016) 109–117, https://doi.org/10.3329/jsr.v8i2.25057.

[48] M.R. Khatun, M.A. Ali, F. Parvin, A.K.M.A. Islam, Elastic, thermodynamic and optical behavior of V 2 A C (A = Al, Ga) MAX phases, Results Phys. 7 (2017) 3634–3639, https://doi.org/10.1016/j.rinp.2017.09.043.

[49] M. Akhter, M.S. Ahasan, M.A. Ali, F. Parvin, Elastic, electronic, optical, and thermodynamic properties of M2SeC (M = Hf, Zr) under high pressure, AIP Adv. 13 (2023), https://doi.org/10.1063/5.0136222.

[50] M. Roknuzzaman, M.A. Hadi, M.A. Ali, M.M. Hossain, N. Jahan, M.M. Uddin, J.A. Alarco, K. Ostrikov, First hafnium-based MAX phase in the 312 family, Hf 3 AlC 2 : A first-principles study, J. Alloys Compd. 727 (2017) 616–626. doi:https://doi.org/10.1016/j.jallcom.2017.08.151.

[51] M.A. Ali, M.M. Hossain, N. Jahan, A.K.M.A. Islam, S.H. Naqib, Newly synthesized Zr 2 AlC, Zr 2 (Al 0.58 Bi 0.42)C, Zr 2 (Al 0.2 Sn 0.8)C, and Zr 2 (Al 0.3 Sb 0.7)C MAX phases: A DFT based first-principles study, Comput. Mater. Sci. 131 (2017) 139–145. doi:https://doi.org/10.1016/j.commatsci.2017.01.048.

[52] M.A. Ali, M.M. Hossain, M.A. Hossain, M.T. Nasir, M.M. Uddin, M.Z. Hasan, A.K.M. A. Islam, S.H. Naqib, Recently synthesized (Zr 1-x Ti x) 2 AlC ($0 \leq x \leq 1$) solid solutions: theoretical study of the effects of M mixing on physical properties, J. Alloys Compd. 743 (2018) 146–154, https://doi.org/10.1016/j.jallcom.2018.01.396.

[53] Z. Zhang, X. Duan, D. Jia, Y. Zhou, S. van der Zwaag, On the formation mechanisms and properties of MAX phases: a review, J. Eur. Ceram. Soc. 41 (2021) 3851–3878, https://doi.org/10.1016/j.jeurceramsoc.2021.02.002.

[54] M.A. Ali, M.M. Hossain, A.K.M.A. Islam, S.H. Naqib, Ternary boride Hf3PB4: insights into the physical properties of the hardest possible boride MAX phase, J. Alloys Compd. 857 (2021) 158264, https://doi.org/10.1016/j.jallcom.2020.158264.

[55] M. Born, On the stability of crystal lattices. I, Math. Proc. Camb. Philos. Soc. 36 (1940) 160–172, https://doi.org/10.1017/S0305004100017138.

[56] F. Mouhat, F.X. Coudert, Necessary and sufficient elastic stability conditions in various crystal systems, Phys. Rev. B - Condens. Matter Mater. Phys. 90 (2014) 224104, https://doi.org/10.1103/PhysRevB.90.224104.

[57] R. Hill, First-principles elastic constants for the hcp transition metals Fe, Co, and Re at high pressure, in: Proc. Phys. Soc, 1952: p. 350.

[58] W. Voigt, Lehrbuch der Kristallphysik, Lehrbuch der Kristallphysik, 1928.

[59] A. Reuss, ZAMM-journal of applied mathematics and mechanics, Zeitschrift Fur Angew. Math. Und Mech. 9 (1929) 49.

[60] M.A. Ali, N. Jahan, A.K.M.A. Islam, Sulvanite compounds Cu_3TMS_4 (TM = V, Nb and ta): elastic, electronic, optical and thermal properties using first-principles method, J. Sci. Res. 6 (2014) 407–419, https://doi.org/10.3329/jsr.v6i3.19191.

[61] A. Bouhemadou, Calculated structural, electronic and elastic properties of M2GeC (M=Ti, V, Cr, Zr, Nb, Mo, Hf, ta and W), Appl. Phys. A Mater. Sci. Process. 96 (2009) 959–967, https://doi.org/10.1007/s00339-009-5106-5.

[62] M. Atikur Rahman, Study on Structural, Electronic, Optical and Mechanical Properties of MAX Phase Compounds and Applications Review Article, Am, J. Mod. Phys. 4 (2015) 75, https://doi.org/10.11648/j.ajmp.20150402.15.

[63] M. Sohel, M.M. Uddin, M.A. Ali, M.M. Hossain, A.K.M.A. Islam, S.H. Naqib, Impact of M atomic species on physical properties of M2TlC (M = Ti, Zr, Hf): a first principles calculation, AIP Adv. 13 (2023), https://doi.org/10.1063/5.0150252.

[64] H. Tian, X. He, J. Wang, H. Meng, L. Shen, L. Wu, D. Qi, Q. Li, P. An, Z. Peng, X. Zhang, C. Bai, Q. Huang, S. Du, Theoretical insights into the physical properties of a new 211 MAX phase V2ZnC under high pressure, Comput. Mater. Sci. 232 (2024) 112649, https://doi.org/10.1016/j.commatsci.2023.112649.

[65] S.F. Pugh, XCII. Relations between the elastic moduli and the plastic properties of polycrystalline pure metals, London, Edinburgh, Dublin Philos. Mag. J. Sci. 45 (1954) 823–843. doi:https://doi.org/10.1080/14786440808520496.

[66] I.N. Frantsevich, Elastic constants and elastic moduli of metals and insulators, Ref. B. (1982).

[67] P. Das, N. Jahan, M.A. Ali, DFT insights into Nb-based 211 MAX phase carbides: Nb 2 AC (a = Ga, Ge, Tl, Zn, P, in, and cd), RSC Adv. 13 (2023) 5538–5556, https://doi.org/10.1039/D2RA07468K.

[68] O.L. Anderson, H.H. Demarest, Elastic constants of the central force model for cubic structures: polycrystalline aggregates and instabilities, J. Geophys. Res. 76 (1971) 1349–1369, https://doi.org/10.1029/jb076i005p01349.

[69] A. Savin, H.-J. Flad, J. Flad, H. Preuss, H.G. von Schnering, On the bonding in Carbosilanes, Angew. Chemie Int. Ed. English 31 (1992) 185–187, https://doi.org/10.1002/anie.199201851.

[70] Z. Sun, D. Music, R. Ahuja, J.M. Schneider, Theoretical investigation of the bonding and elastic properties of nanolayered ternary nitrides, Phys. Rev. B 71 (2005) 193402, https://doi.org/10.1103/PhysRevB.71.193402.

[71] M.F. Cover, O. Warschkow, M.M.M. Bilek, D.R. McKenzie, A comprehensive survey of M 2 AX phase elastic properties, J. Phys. Condens. Matter 21 (2009) 305403, https://doi.org/10.1088/0953-8984/21/30/305403.

[72] S.-R.G. Christopoulos, P.P. Filippatos, M.A. Hadi, N. Kelaidis, M.E. Fitzpatrick, A. Chroneos, Intrinsic defect processes and elastic properties of Ti 3 AC 2 (a = Al, Si, Ga, Ge, in, Sn) MAX phases, J. Appl. Phys. 123 (2018) 025103, https://doi.org/10.1063/1.5011374.

[73] M.A. Hadi, S.R.G. Christopoulos, S.H. Naqib, A. Chroneos, M.E. Fitzpatrick, A.K.M. A. Islam, Physical properties and defect processes of M3SnC2 (M = Ti, Zr, Hf) MAX phases: effect of M-elements, J. Alloys Compd. 748 (2018) 804–813, https://doi.org/10.1016/j.jallcom.2018.03.182.

[74] F. Gao, Theoretical model of intrinsic hardness, Phys. Rev. B 73 (2006) 132104, https://doi.org/10.1103/PhysRevB.73.132104.

[75] H. Gou, L. Hou, J. Zhang, F. Gao, Pressure-induced incompressibility of ReC and effect of metallic bonding on its hardness, Appl. Phys. Lett. 92 (2008) 241901, https://doi.org/10.1063/1.2938031.

[76] M.T. Nasir, M.A. Hadi, M.A. Rayhan, M.A. Ali, M.M. Hossain, M. Roknuzzaman, S. H. Naqib, A.K.M.A. Islam, M.M. Uddin, K. Ostrikov, First-principles study of superconducting ScRhP and ScIrP pnictides, Phys. Status Solidi 254 (2017) 1700336, https://doi.org/10.1002/pssb.201700336.

[77] H.M. Ledbetter, Elastic properties of zinc: a compilation and a review, J. Phys. Chem. Ref. Data Monogr. 6 (1977) 1181–1203, https://doi.org/10.1063/1.555564.

[78] J. Gonzalez-Julian, Processing of MAX phases: from synthesis to applications, J. Am. Ceram. Soc. 104 (2021) 659–690, https://doi.org/10.1111/jace.17544.

[79] S. Islam, M.R. Rana, P. Das, K. Hoque, S.H. Naqib, M.A. Ali, DFT insights into i-MAB phase, Mo 4 Y 2 Al 3 B 6 : a potential thermal barrier coating and solar heat reducing material, Phys. Scr. 99 (2024) 055975. doi:https://doi.org/10.1088/1402-4896/ad3d90.

[80] O.L. Anderson, A simplified method for calculating the debye temperature from elastic constants, J. Phys. Chem. Solid 24 (1963) 909–917, https://doi.org/10.1016/0022-3697(63)90067-2.

[81] M.E.A. Belhadj, M. Berrahal, A. Bentouaf, M. Belmekki, M.E.A. Elaissaoui El Meliani, F. Benaddi, A. Azzouz Rached, Structural parameters, electronic structure, magnetic, and mechanical properties of half-metallic full-Heusler compound Cr2VAs: a density functional theory study, Comput. Theor. Chem. 1234 (2024) 114526, https://doi.org/10.1016/j.comptc.2024.114526.

[82] M.R. Rana, S. Islam, K. Hoque, S. Mahmud, M.A. Ali, Newly synthesized Pb-based 312 MAX phases M3PbC2 (M = Zr and Hf): a first-principles study, Diamond Relat. Mater. 146 (2024) 111245, https://doi.org/10.1016/j.diamond.2024.111245.

[83] M.A. Rayhan, M.A. Ali, S.H. Naqib, A.K.M.A. Islam, First-principles study of Vickers hardness and thermodynamic properties of Ti_3SnC_2 polymorphs, J. Sci. Res. 7 (2015) 53–64, https://doi.org/10.3329/jsr.v7i3.23182.

[84] G.A. Slack, The Thermal Conductivity of Nonmetallic Crystals, in: Solid State Phys. - Adv. Res. Appl., 1979: pp. 1–71. doi:https://doi.org/10.1016/S0081-1947(08)60359-8.

[85] S. Li, W. Sun, Y. Luo, J. Yu, L. Sun, B.-T. Wang, J.-X. Liu, G.-J. Zhang, I. Di Marco, Pushing the limit of thermal conductivity of MAX borides and MABs, J. Mater. Sci. Technol. 97 (2022) 79–88, https://doi.org/10.1016/J.JMST.2021.05.006.

[86] G.A. Slack, The thermal conductivity of nonmetallic crystals, solid state Phys. - Adv, Res. Appl. 34 (1979) 1–71, https://doi.org/10.1016/S0081-1947(08)60359-8.

[87] B. Liu, Y. Liu, C. Zhu, H. Xiang, H. Chen, L. Sun, Y. Gao, Y. Zhou, Advances on strategies for searching for next generation thermal barrier coating materials, J. Mater. Sci. Technol. 35 (2019) 833–851, https://doi.org/10.1016/j.jmst.2018.11.016.
[88] M.A. Hadi, N. Kelaidis, S.H. Naqib, A. Chroneos, A.K.M.A. Islam, Mechanical behaviors, lattice thermal conductivity and vibrational properties of a new MAX phase Lu2SnC, J. Phys. Chem. Solid 129 (2019) 162–171, https://doi.org/10.1016/j.jpcs.2019.01.009.
[89] M.A. Blanco, E. Francisco, V. Luaña, GIBBS: isothermal-isobaric thermodynamics of solids from energy curves using a quasi-harmonic Debye model, Comput. Phys. Commun. 158 (2004) 57–72, https://doi.org/10.1016/j.comphy.2003.12.001.
[90] S. Li, R. Ahuja, M.W. Barsoum, P. Jena, B. Johansson, Optical properties of Ti3SiC2 and Ti 4AlN3, Appl. Phys. Lett. 92 (2008) 90–93, https://doi.org/10.1063/1.2938862.
[91] M.M. Hossain, M.A. Ali, M.M. Uddin, S.H. Naqib, A.K.M.A. Islam, Newly synthesized three-dimensional boron-rich chalcogenides B 12 X (X = S and se): theoretical characterization of the physical properties for optoelectronic and mechanical applications, ACS Omega 6 (2021) 33899–33913, https://doi.org/10.1021/acsomega.1c05172.
[92] M.M. Hossain, M.A. Hossain, S.A. Moon, M.A. Ali, M.M. Uddin, S.H. Naqib, A.K.M. A. Islam, M. Nagao, S. Watauchi, I. Tanaka, NaInX2 (X = S, se) layered materials for energy harvesting applications: first-principles insights into optoelectronic and thermoelectric properties, J. Mater. Sci. Mater. Electron. 32 (2021) 3878–3893, https://doi.org/10.1007/s10854-020-05131-7.
[93] A. Chowdhury, M.A. Ali, M.M. Hossain, M.M. Uddin, S.H. Naqib, A.K.M.A. Islam, Predicted MAX phase Sc2InC: dynamical stability, vibrational and optical properties, Phys. Status Solidi Basic Res. 255 (2018) 1–9, https://doi.org/10.1002/pssb.201700235.
[94] M.A. Ali, M.S. Ali, M.M. Uddin, Structural, elastic, electronic and optical properties of metastable MAX phase Ti5SiC4 compound, Indian J. Pure Appl. Phys. 54 (2016) 386–390.
[95] M.A. Hadi, M. Dahlqvist, S.R.G. Christopoulos, S.H. Naqib, A. Chroneos, A.K.M. A. Islam, Chemically stable new MAX phase V2SnC: a damage and radiation tolerant TBC material, RSC Adv. 10 (2020) 43783–43798, https://doi.org/10.1039/d0ra07730e.